01 Feb 2022

A Multigrid Multilevel Monte Carlo Method for Stokes–Darcy Model with Random Hydraulic Conductivity and Beavers–Joseph Condition

Zhipeng Yang

Ju Ming

Changxin Qiu

Maojun Li

et. al. For a complete list of authors, see https://scholarsmine.mst.edu/math_stat_facwork/1178

A Multigrid Multilevel Monte Carlo Method for Stokes–Darcy Model with Random Hydraulic Conductivity and Beavers–Joseph Condition

Zhipeng Yang[1,2] · Ju Ming[3] · Changxin Qiu[4] · Maojun Li[5] · Xiaoming He[6]

Abstract

A multigrid multilevel Monte Carlo (MGMLMC) method is developed for the stochastic Stokes–Darcy interface model with random hydraulic conductivity both in the porous media domain and on the interface. Three interface conditions with randomness are considered on the interface between Stokes and Darcy equations, especially the Beavers–Joesph interface condition with random hydraulic conductivity. Because the randomness through the interface affects the flow in the Stokes domain, we investigate the coupled stochastic Stokes–Darcy model to improve the fidelity. Under suitable assumptions on the random coefficient, we prove the existence and uniqueness of the weak solution of the variational form. To construct the numerical method, we first adopt the Monte Carlo (MC) method and finite element method, for the discretization in the probability space and physical space, respectively. In order to improve the efficiency of the classical single-level Monte Carlo (SLMC) method, we adopt the multilevel Monte Carlo (MLMC) method to dramatically reduce the computational cost in the probability space. A strategy is developed to calculate the number of samples needed in MLMC method for the stochastic Stokes–Darcy model. In order to accomplish the strategy for MLMC method, we also present a practical method to determine the variance convergence rate for the stochastic Stokes–Darcy model with Beavers–Joseph interface condition. Furthermore, MLMC method naturally provides the hierarchical grids and sufficient information on these grids for multigrid (MG) method, which can in turn improve the efficiency of MLMC method. In order to fully make use of the dynamical interaction between this two methods, we propose a multigrid multilevel Monte Carlo (MGMLMC) method with finite element discretization for more efficiently solving the stochastic model, while additional attention is paid to the interface and the random Beavers–Joesph interface condition. The computational cost of the proposed MGMLMC method is rigorously analyzed and compared with the SLMC method. Numerical examples are provided to verify and illustrate the proposed method and the theoretical conclusions.

Keywords Stochastic Stokes–Darcy interface model · Beavers–Joseph interface condition · Multilevel Monte Carlo · Multigrid method · Finite elements

Extended author information available on the last page of the article

Mathematics Subject Classification 35R60 · 65C05 · 65M60 · 76S05

1 Introduction

The Stokes–Darcy interface model has attracted significant attention from scientists and engineers due to its wide range of applications, such as interaction between surface and subsurface flows [25,36,38,67,78], industrial filtrations [45,64], groundwater system in karst aquifers [24,50,62,63], petroleum extraction [2,42,61,85,122], and many others [26,28,34,35,84,100,105,110,124]. Therefore it is not surprising that many different numerical methods have been proposed and analyzed for the Stokes–Darcy model, including domain decomposition methods [14,20,22,30,37,39,40,60,109], Lagrange multiplier methods [4,51,79], discontinuous Galerkin methods [32,57,71,82,97], multigrid methods [1,18,87], partitioned time stepping methods [74,88,103,121], coupled finite element methods [3,19,72,86,101], and many others [8,13,31,44,48,58,65,69,70,81,89,102,112,114].

The above existing works only consider the deterministic Stokes–Darcy model, for which the problem data, including the model coefficients, the forcing terms, the domain geometry, the boundary conditions and the initial conditions, are assumed to be perfectly known. However, in reality there is a significant amount of uncertainty involved in determining these real-life data due to measurements and simplifications [33,52,91,104]. Up to the authors' knowledge, in the literature there is only one existing pioneer work [76] which considers the stochastic transport problem of Stokes–Darcy model with Beavers–Joseph–Saffmann interface condition.

In recent years, various numerical methods have been developed to solve stochastic partial differential equations, such as the polynomial chaos methods [117,118], the collocation methods [5,6], the sparse grid methods [9,92,93], and many others [7,65,94,111,115,116, 119,123,125]. There also exist many works on the uncertainties of the porous media flow by assuming the hydraulic conductivity of the porous media is a random field in the second order elliptic equation [41,49,80,120]. But the Stokes–Darcy model has a much more complicated system for the uncertainties due to the flow interaction on the interface between the porous media flow and the free flow in conduits.

Therefore, it is not trivial to study the effect of randomness of the hydraulic conductivity on the whole coupled flow performance, which is key component of this paper, especially around the interface. Furthermore, most of the existing works on Stokes–Darcy model consider the simplified Beavers–Joseph–Saffmann interface condition, including the pioneer work [76] for the stochastic transport problem of Stokes–Darcy model. In this paper, we will consider the original Beavers–Joseph interface condition [12], which is more complicated and brings more difficulties [21,23]. Starting from the analysis for the wellposedness of the stochastic Stokes–Darcy model with random Beavers–Joseph condition, we will develop the proposed method step by step, by following and improving the ideas of the multigrid multilevel Monte Carlo (MGMLMC) method in [76].

The Monte Carlo method [99] is widely used in a range of stochastic problems, owing to the dimension independent convergence rate of the sampling error. However, high accuracies of Monte Carlo method require a large number of samples, and the convergence is determined by the number of the samplings under the Central Limit Theorem. Then the performance of Monte Carlo method for the stochastic partial differential equations on a fine mesh will lead to very expensive computational cost. To reduce the computational cost for simulating the coupled stochastic Stokes–Darcy model, we adopt the multilevel Monte Carlo method, which

is an effective variance reduction method. This method is introduced by M. Giles [53,54], and has been used in many research works [11,27,43,55,77,107]. It is much more costly efficient by significantly reducing the number of samples on the fine meshes.

However, it is not trivial to determine the number of samples in each level to keep the global accuracy while minimizing the cost. Therefore, motivated by the idea in [75], in this paper we particularly develop a strategy based on a detailed analysis to overcome this difficulty for the stochastic Stokes–Darcy model with random Beavers–Joseph interface condition. To perform this strategy, we also provide a suitable method to determine the variance convergence rate for calculating the number of samples needed in MLMC method.

Furthermore, the multilevel Monte Carlo method only reduces the computational cost in the probability space, not in the physical space. Inspired by a fact that the multilevel Monte Carlo method already has a set of hierarchical grids for the multilevel idea, it is a natural idea to fully make use of the same set of hierarchical grids to solve the discrete algebraic system by using the powerful multigrid method [15,17,108], which can further improve the efficiency of the proposed multilevel Monte Carlo method. Meanwhile, the saved information of the multilevel Monte Carlo method on the set of hierarchical grids will also significantly reduce the computational cost of the multigrid method.

Therefore, we adopt the multigrid multilevel Monte Carlo (MGMLMC) method, which combines the multilevel Monte Carlo method and the multigrid method on the same set of hierarchical grids to propose an even more costly efficient method. The MGMLMC method has been developed for various models, such as the stochastic elliptic variational inequalities [73], the stochastic elliptic equations [98], the lognormal diffusion problems [75], and the transport in Stokes–Darcy system [76]. Particularly, the finite volume method was used for the spatial discretization in [76] to solve the transport model, whose velocity field is obtained from the coupled Stokes–Darcy equation with the Beaver-Joseph-Saffmann interface condition.

In this paper, we develop the MGMLMC method for the stochastic Stokes–Darcy model with the random Beavers–Joseph interface condition. The randomness in the original Beavers–Joseph interface condition, which is more complicated than the simplified Beaver-Joseph-Saffmann interface condition, brings more difficulties to the model. In the proposed method, finite elements are utilized for the physical space discretization, and the grid based method [59] is adopted to generate the realizations of the random hydraulic conductivity in the probability space. Furthermore, the computational cost of the proposed MGMLMC method is rigorously analyzed and compared with the SLMC method for the stochastic Stokes–Darcy model with the random Beavers–Joseph condition.

The rest of the paper is organized as follows. In Sect. 2, we briefly recall the deterministic Stokes–Darcy model. In Sect. 3, we present the stochastic Stokes–Darcy interface model, the weak formulation of the stochastic Stokes–Darcy model and the proof of the wellposedness. In Sect. 4, we recall the Monte Carlo method to approximate the numerical moments of the stochastic solutions, adopt the multilevel Monte Carlo method to reduce the computational cost in probability space, and then develop the multigrid multilevel Monte Carlo to further reduce the computational cost. In Sect. 5 we provide numerical examples to verify the theoretical analysis and illustrate the features of the proposed methods.

2 Deterministic Model for Coupled Porous Media Flow with Fluid Flow

The coupled Stokes–Darcy system describes the confined flow by Darcy system in the porous media domain and the free flow by Stokes equations in the conduit domain. Then three

interface conditions are used to couple the flows in these two domains. In this paper, we consider the coupled Stokes–Darcy system on a bounded domain $D_{ms} = D_m \cup D_s \subset \mathbb{R}^d$, $d = 2, 3$, where D_m is the porous media domain and D_s is the conduit domain. We decompose the boundary ∂D_{ms} into two parts: $\Gamma_m = \partial D_m \backslash \Gamma_I$, $\Gamma_s = \partial D_s \backslash \Gamma_I$, and denote the interface as $\Gamma_I = \partial D_m \cap \partial D_s$.

In the porous media domain D_m, the flow is governed by the Darcy system [10]

$$\mathbf{u}_m(x) = -\mathbb{K}(x)\nabla\phi_m(x), \quad \text{in } D_m, \tag{1}$$

$$\nabla \cdot \mathbf{u}_m(x) = f_m(x), \quad \text{in } D_m, \tag{2}$$

here, $\mathbf{u}_m$ denotes the specific discharge in the porous media, $\mathbb{K}$ is the hydraulic conductivity tensor of the porous media that is symmetric and positive definite in accordance with physical meaning, ϕ_m is the hydraulic head, and f_m is the sink/source term.

By substituting (1) into (2), we obtain the second-order form of the Darcy system

$$-\nabla \cdot (\mathbb{K}(x)\nabla\phi_m(x)) = f_m(x), \quad \text{in } D_m. \tag{3}$$

In the conduit domain D_s, the flow is governed by the Stokes equations:

$$-\nabla \cdot \mathbb{T}(\mathbf{u}_s, p_s) = \mathbf{f}_s, \quad \text{in } D_s, \tag{4}$$

$$\nabla \cdot \mathbf{u}_s = 0, \quad \text{in } D_s, \tag{5}$$

where $\mathbf{u}_s$ denotes the fluid velocity, p_s is the kinematic pressure, and $\mathbf{f_s}$ is the external body force. $\mathbb{T}$ is the stress tensor, defined as $\mathbb{T}(\mathbf{u}_s, p_s) = 2\nu\mathbb{D}(\mathbf{u}_s) - p_s\mathbb{I}$, where ν is the kinematic viscosity of the fluid, $\mathbb{I}$ is the identity matrix, and $\mathbb{D}(\mathbf{u}_s) = \frac{1}{2}(\nabla\mathbf{u}_s + (\nabla\mathbf{u}_s)^T)$.

On the interface between the porous media domain and the conduit domain, we impose three interface conditions:

$$\mathbf{u}_s \cdot \mathbf{n}_s = (\mathbb{K}\nabla\phi_m) \cdot \mathbf{n}_m, \quad \text{on } \Gamma_I, \tag{6}$$

$$-\mathbf{n}_s^\top \mathbb{T}(\mathbf{u}_s, p_s)\mathbf{n}_s = g(\phi_m - z), \quad \text{on } \Gamma_I, \tag{7}$$

$$-\boldsymbol{\tau}_j^\top \mathbb{T}(\mathbf{u}_s, p_s)\mathbf{n}_s = \frac{\alpha\nu\sqrt{d}}{\sqrt{\text{trace}(\Pi(x))}}\boldsymbol{\tau}_j^\top(\mathbf{u}_s + \mathbb{K}\nabla\phi_m), \quad \text{on } \Gamma_I, \tag{8}$$

where $\mathbf{n}_m$, $\mathbf{n}_s$ denote the unit outer normal to the porous media and the conduit regions at the interface Γ_I, respectively, $\boldsymbol{\tau}_j(j = 1, \ldots, d - 1)$ denote mutually orthogonal unit tangential vectors to the interface Γ_I, z is the hight, g is the gravitational acceleration, and $\Pi(x) = \frac{\mathbb{K}(x)\nu}{g}$ is the intrinsic permeability. The first interface condition (6) is governed by the conservation of mass, the second interface condition (7) represents the balance of the kinematic pressure in the matrix and the stress in the free flow at the normal direction along the interface, and the last interface condition (8) is the famous Beavers–Joseph condition [12,21,23,24,47,66,68,83,95,103].

3 Stokes–Darcy Interface Model with Random Permeability

To overcome the difficulty of measuring the exact permeability at every point in the porous media domain, we use an underlying random field to describe the intrinsic permeability tensor Π. Thus the hydraulic conductivity tensor $\mathbb{K}(x)$ is also a random field with the relationship $\mathbb{K} = \frac{g\Pi}{\nu}$. Then we obtain the stochastic partial differential equations to describe the coupled system with the random hydraulic conductivity, based on the deterministic model in the above section. In this paper, we will investigate the uncertainty in the porous domain and

the uncertainty transferred to the conduit domain through the interface. In this section, we will provide the weak formulation and prove the wellposedness of the weak solution of the coupled stochastic model.

3.1 Functional Spaces and Notations

Before the study of the stochastic coupled problem, we introduce some notations. Throughout this paper, we adopt the notations in [46] for the classical Sobolev spaces. Let D be an open, connected, bounded, and convex subset of $\mathbb{R}^d$, $d = 2, 3$, with polygonal and Lipschitz continuous boundary ∂D. Following the notations in [46], let $r \in \mathbb{R}$, $q \in \mathbb{Z}$, and $W^{r,q}(D)$ be a deterministic Sobolev space on D with the standard norm $\| \cdot \|_{W^{r,q}(D)}$ and semi-norm $| \cdot |_{W^{r,q}(D)}$. For $q = 2$, define the Hilbert space $H^r(D) := W^{r,2}(D)$ and $H_0^r(D) := \{u : u \in H^r(D), u \mid_{\partial D} = 0\}$ with the standard norm $\| \cdot \|_{H^r(D)}$ and semi-norm $| \cdot |_{H^r(D)}$. For $d = 2, 3$, define $\mathbf{H}^r(D) := (H^r(D))^d$ and $\mathbf{L}^q(D) := (L^q(D))^d$. For the vector $\mathbf{v} = (v_1, v_2, \ldots, v_n)^\top$, $n \in \mathbb{N}^+$, 2-norm $\| \cdot \|_2$ of $\mathbf{v}$ is $\|\mathbf{v}\|_2 = \left(v_1^2 + v_2^2 + \cdots + v_n^2\right)^{1/2}$.

Then we define the stochastic Sobolev space. Let $(\Omega, \mathcal{F}, \mathcal{P})$ be a complete probability space. Here Ω is the set of outcomes, $\mathcal{F}$ is the σ-algebra of events, and $\mathcal{P} : \mathcal{F} \to [0, 1]$ is a probability measure. Then the stochastic Sobolev space, which consists of strongly measurable, r-summable mappings $\phi : \Omega \to W^{r,q}(D)$, is denoted as

$$L^2\left(\Omega; W^{r,q}(D)\right) := \{\phi : \Omega \to W^{r,q}(D) \mid \phi \text{ strongly measurable, } \|\phi\|_{L^2(\Omega; W^{r,q}(D))} < \infty\}.$$

Here $\| \cdot \|_{L^2(\Omega; W^{r,q}(D))}$ is the norm given as, $\forall \phi \in L^2\left(\Omega; W^{r,q}(D)\right)$,

$$\|\phi\|_{L^2(\Omega; W^{r,q}(D))} := \left(\mathbb{E}\left[\|\phi(\omega, \cdot)\|_{W^{r,q}(D)}^2\right]\right)^{1/2} := \left(\int_\Omega \|\phi(\omega, \cdot)\|_{W^{r,q}(D)}^2 d\mathcal{P}(\omega)\right)^{1/2},$$

which is induced by following inner product, $\forall \phi, \psi \in L^2(\Omega; W^{r,q}(D))$,

$$[\phi, \psi]_{L^2(\Omega; W^{r,q}(D))} := \mathbb{E}\left[(\phi, \psi)_{W^{r,q}(D)}\right] := \int_\Omega (\phi, \psi)_{W^{r,q}(D)} d\mathcal{P}(\omega).$$

For simplicity, we define

$$\mathcal{L}^q(D) = L^2(\Omega; L^q(D)), \text{ with norm } \| \cdot \|_{\mathcal{L}^q(D)} = \| \cdot \|_{L^2(\Omega; L^q(D))},$$
$$\mathcal{H}^r(D) = L^2(\Omega; H^r(D)), \text{ with norm } \| \cdot \|_{\mathcal{H}^r(D)} = \| \cdot \|_{L^2(\Omega; H^r(D))},$$
$$\boldsymbol{\mathcal{L}}^q(D) = L^2(\Omega; \mathbf{L}^q(D)), \text{ with norm } \| \cdot \|_{\boldsymbol{\mathcal{L}}^q(D)} = \| \cdot \|_{L^2(\Omega; \mathbf{L}^q(D))},$$
$$\boldsymbol{\mathcal{H}}^r(D) = L^2(\Omega; \mathbf{H}^r(D)), \text{ with norm } \| \cdot \|_{\boldsymbol{\mathcal{H}}^r(D)} = \| \cdot \|_{L^2(\Omega; \mathbf{H}^r(D))}.$$

3.2 Stochastic Stokes–Darcy Interface Equations

With the complete probability space $(\Omega, \mathcal{F}, \mathcal{P})$, let $\mathbb{K}(\omega, x)$, $\omega \in \Omega$, $x \in \bar{D}_m$ be a random hydraulic conductivity tensor. Then in the porous media domain, the stochastic second-order form of Darcy equation with deterministic sink/source term $f_m(x)$ is given as:

$$-\nabla \cdot \left(\mathbb{K}(\omega, x)\nabla \phi_m(\omega, x)\right) = f_m(x), \quad \text{in } D_m. \tag{9}$$

And the interface conditions on Γ_I with random hydraulic conductivity are

$$\mathbf{u}_s(\omega, x) \cdot \mathbf{n}_s(x) = \big(\mathbb{K}(\omega, x)\nabla\phi_m(\omega, x)\big) \cdot \mathbf{n}_m(x), \tag{10}$$

$$-\mathbf{n}_s^\top \mathbb{T}(\mathbf{u}_s, p_s)\mathbf{n}_s = g(\phi_m(\omega, x) - z), \tag{11}$$

$$-\boldsymbol{\tau}_j^\top \mathbb{T}(\mathbf{u}_s, p_s)\mathbf{n}_s = \frac{\alpha v\sqrt{d}}{\sqrt{\mathrm{trace}(\Pi(\omega, x))}} \boldsymbol{\tau}_j^\top \big(\mathbf{u}_s(\omega, x) + \mathbb{K}(\omega, x)\nabla\phi_m(\omega, x)\big). \tag{12}$$

Due to the randomness transferred from porous media domain through the interface conditions, the Stokes equations in the conduit domain become stochastic as follows

$$-\nabla \cdot \mathbb{T}(\mathbf{u}_s(\omega, x), p_s(\omega, x)) = \mathbf{f}_s(x), \quad \text{in } D_s, \tag{13}$$

$$\nabla \cdot \mathbf{u}_s(\omega, x) = 0, \quad \text{in } D_s. \tag{14}$$

For the boundary conditions, we assume the hydraulic head ϕ_m and the fluid velocity $\mathbf{u}_s$ satisfy deterministic homogeneous Dirichlet boundary condition except on Γ_I.

3.3 Weak Formulation of the Coupled Problem

We denote the pressure spaces on the porous media as

$$X_m = \{\phi_m \in \mathcal{H}^1(D_m) \mid \phi_m = 0 \text{ on } \Gamma_m\},$$
$$X_m^0 = \{\phi_m \in \mathcal{H}^0(D_m) \mid \phi_m = 0 \text{ on } \Gamma_m\},$$

and the velocity-pressure spaces on the conduit domain as

$$X_s = \{\mathbf{u}_s \in \mathcal{H}^1(D_s) \mid \mathbf{u}_s = 0 \text{ on } \Gamma_s\},$$
$$X_s^0 = \{\mathbf{u}_s \in \mathcal{H}^0(D_s) \mid \mathbf{u}_s = 0 \text{ on } \Gamma_s\},$$
$$X_{s,div} = \{\mathbf{u}_s \in X_s \mid \nabla \cdot \mathbf{u}_s = 0 \text{ in } D_s\},$$
$$Q_s = \{q_s \in \mathcal{L}^2(D_s)\}.$$

For convenience, let $X^1 = X = X_m \times X_s$, $X_{div} = X_m \times X_{s,div}$, $X^0 = X_m^0 \times X_s^0$, and $\underline{u} = (\phi_m, \mathbf{u}_s) \in X$, where $\phi_m \in X_m$, $\mathbf{u}_s \in X_s$. The norms of $X^r, r = 0, 1$ are given as

$$\|\underline{u}\|_{X^r} = \left(\mathbb{E}\Big[\|\underline{u}\|_{H^r(D_m)\times\mathbf{H}^r(D_s)}^2\Big]\right)^{1/2} = \left(\|\phi_m\|_{\mathcal{H}^r(D_m)}^2 + \|\mathbf{u}_s\|_{\mathcal{H}^r(D_s)}^2\right)^{1/2}. \tag{15}$$

The projection onto the local tangential plane of the vector $\mathbf{u}$ is denoted as $P_\tau(\mathbf{u}) = \mathbf{u} - (\mathbf{u} \cdot \mathbf{n}_s)\mathbf{n}_s$. Then using the boundary conditions (10)-(12), we obtain the following weak formulation: find $(\underline{u}, p_s) \in X \times Q_s$, such that

$$\begin{cases} A(\underline{u}, \underline{v}) - B(\underline{v}, p_s) = F(\underline{v}), & \forall \underline{v} = (\psi_m, \mathbf{v}_s) \in X, \\ B(\underline{u}, q_s) = 0, & \forall q_s \in Q_s, \end{cases} \tag{16}$$

where

$$A(\underline{u}, \underline{v}) = \mathbb{E}\left[a(\underline{u}, \underline{v})\right] = \int_{\Omega} a(\underline{u}, \underline{v}) d\omega, \tag{17}$$

$$a(\underline{u}, \underline{v}) = \int_{D_s} 2\nu \mathbb{D}(\mathbf{u}_s) : \mathbb{D}(\mathbf{v}_s) dx + g \int_{D_m} (\mathbb{K}\nabla\phi_m) \cdot \nabla\psi_m dx \tag{18}$$

$$+ g \int_{\Gamma_I} \phi_m \mathbf{v}_s \cdot \mathbf{n}_s d\Gamma_I + \int_{\Gamma_I} \frac{\alpha\nu\sqrt{d}}{\sqrt{\mathrm{trace}(\Pi)}} P_\tau(\mathbb{K}\nabla\phi_m) \cdot \mathbf{v}_s d\Gamma_I \tag{19}$$

$$- g \int_{\Gamma_I} (\mathbf{u}_s \cdot \mathbf{n}_s)\psi_m d\Gamma_I + \int_{\Gamma_I} \frac{\alpha\nu\sqrt{d}}{\sqrt{\mathrm{trace}(\Pi)}} P_\tau(\mathbf{u}_s) \cdot \mathbf{v}_s d\Gamma_I, \tag{20}$$

$$B(\underline{v}, p_s) = \mathbb{E}\left[b(\underline{v}, p_s)\right] = \int_{\Omega} b(\underline{v}, p_s) d\omega, \tag{21}$$

$$b(\underline{v}, p_s) = \int_{D_s} p_s \nabla \cdot \mathbf{v}_s dx, \tag{22}$$

$$F(\underline{v}) = \mathbb{E}\left[f(\underline{v})\right] = \int_{\Omega} f(\underline{v}) d\omega, \tag{23}$$

$$f(\underline{v}) = \int_{D_s} \mathbf{f}_s \cdot \mathbf{v}_s dx + g \int_{D_m} f_m \psi_m dx + \int_{\Gamma_I} gz\mathbf{v}_s \cdot \mathbf{n}_s d\Gamma_I. \tag{24}$$

3.4 Wellposedness of the Weak Solution

The approach to analyze the wellposedness in our paper follows the ideas in [11,24,56,96]. To ensure the existence and uniqueness of the weak solution, $\mathbb{K}(\omega, x)$ is assumed to be a diagonal matrix as $\mathrm{diag}\left(K_{11}(\omega, x), \ldots, K_{dd}(\omega, x)\right)$, $\omega \in \Omega$, $x \in \bar{D}_m = D_m \cup \partial D_m$, $d = 2, 3$, and satisfy the strong elliptic condition that there are positive lower and upper bounds K_{min}, K_{max} such that

$$0 < K_{min} \leq \left\{K_{ii}(\omega, x)\right\}_{i=1}^{d} \leq K_{max} < \infty, \text{ for } (\omega, x) \in \Omega \times \bar{D}_m. \tag{25}$$

Then several properties of the weak formulation can be derived.

Lemma 1 *With the assumption* (25)*, the bilinear form $A(\cdot, \cdot)$ is continuous on $X_{div} \times X_{div}$.*

Proof By using the Cauchy–Schwarz inequality, trace theorem and (25), we have

$$\begin{aligned} A(\underline{u}, \underline{v}) \leq &2\nu \|\mathbf{u}_s\|_{\mathcal{H}^1(D_s)} \|\mathbf{v}_s\|_{\mathcal{H}^1(D_s)} + gdK_{max} \|\phi_m\|_{\mathcal{H}^1(D_m)} \|\psi_m\|_{\mathcal{H}^1(D_m)} \\ &+ g\|\phi_m\|_{\mathcal{H}^1(D_m)} \|\mathbf{v}_s\|_{\mathcal{H}^1(D_s)} + \frac{\alpha\sqrt{g\nu}}{\sqrt{K_{min}}} \|\mathbf{u}_s\|_{\mathcal{H}^1(D_s)} \|\mathbf{v}_s\|_{\mathcal{H}^1(D_s)} \\ &+ g\|\psi_m\|_{\mathcal{H}^1(D_m)} \|\mathbf{u}_s\|_{\mathcal{H}^1(D_s)} + \frac{\alpha dK_{max}\sqrt{g\nu}}{\sqrt{K_{min}}} \|\phi_m\|_{\mathcal{H}^1(D_m)} \|\mathbf{v}_s\|_{\mathcal{H}^1(D_s)}, \end{aligned}$$

for $\forall \underline{u}, \underline{v} \in X_{div}$. Thus the bilinear form $A(\cdot, \cdot)$ is continuous on the space $X_{div} \times X_{div}$. □

Lemma 2 *The linear form $F(\cdot)$ is continuous on X_{div}.*

Proof By using the Cauchy–Schwarz inequality and trace theorem, we have

$$F(\underline{v}) \leq \|\mathbf{f}_s\|_{\mathcal{H}^1(D_s)} \|\mathbf{v}_s\|_{\mathcal{H}^1(D_s)} + g\|f_m\|_{\mathcal{L}^2(D_m)} \|\psi_m\|_{\mathcal{H}^1(D_m)} + gz\|\mathbf{v}_s\|_{\mathcal{H}^1(D_s)},$$

for $\forall \underline{v} \in X_{div}$. Thus the linear form $F(\cdot)$ is continuous on X_{div}. □

Lemma 3 *With the assumption* (25), *the bilinear form* $A(\cdot, \cdot)$ *is coercive on* $X_{div} \times X_{div}$ *when the coefficient* α *in the Beavers–Joseph condition* (12) *is small enough.*

Proof By using the Korn's inequality, Poincaré inequality, Cauchy–Schwarz inequality, trace theorem and (25), we have

$$
\begin{aligned}
A(\underline{u}, \underline{u}) &= \int_{\Omega} \int_{D_s} 2\nu \mathbb{D}(\mathbf{u}_s) : \mathbb{D}(\mathbf{u}_s) dD_s d\Omega + g \int_{\Omega} \int_{D_m} (\mathbb{K}\nabla\phi_m) \cdot (\nabla\phi_m) dD_m d\Omega \\
&\quad + \int_{\Omega} \int_{\Gamma_I} \frac{\alpha\nu\sqrt{d}}{\sqrt{\operatorname{trace}(\Pi)}} (P_\tau(\mathbf{u}_s) \cdot \mathbf{u}_s + P_\tau(\mathbb{K}\nabla\phi_m) \cdot \mathbf{u}_s) d\Gamma_I d\Omega \\
&\geq 2C_1\nu\|\mathbf{u}_s\|^2_{\mathcal{H}^1(D_s)} + C_2 g K_{min}\|\phi_m\|^2_{\mathcal{H}^1(D_m)} \\
&\quad + \frac{\alpha\sqrt{g\nu}}{\sqrt{K_{max}}}\|P_\tau(\mathbf{u}_s)\|_{\mathcal{L}^2(\Gamma_I)} - \frac{\alpha d K_{max}\sqrt{g\nu}}{\sqrt{K_{min}}}\|\phi_m\|_{\mathcal{H}^1(D_m)}\|\mathbf{u}_s\|_{\mathcal{H}^1(D_s)} \\
&\geq 2C_1\nu\|\mathbf{u}_s\|^2_{\mathcal{H}^1(D_s)} + C_2 g K_{min}\|\phi_m\|^2_{\mathcal{H}^1(D_m)} \\
&\quad - \frac{\alpha d K_{max}\sqrt{g\nu}}{\sqrt{K_{min}}}\|\phi_m\|_{\mathcal{H}^1(D_m)}\|\mathbf{u}_s\|_{\mathcal{H}^1(D_s)} \\
&\geq C_1\nu\|\mathbf{u}_s\|^2_{\mathcal{H}^1(D_s)} + \frac{1}{2}C_2 g K_{min}\|\phi_m\|^2_{\mathcal{H}^1(D_m)},
\end{aligned}
$$

where $\alpha^2 \leq \frac{2C_1 C_2 K_{min}^2}{d^2 K_{max}^2}$, for $\forall \underline{u} \in X_{div}$. Thus the bilinear form $A(\cdot, \cdot)$ is coercive on $X_{div} \times X_{div}$ when the coefficient α in the Beavers–Joseph (12) condition is small enough. $\qquad\square$

Theorem 1 *With the assumption* (25), *there exists a unique weak solution* $\underline{u} = (\mathbf{u}_s, \phi_m) \in X$ *and* p_s *up to an additive constant for the weak formulation* (16) *of stochastic Stoke-Darcy interface problem* (9)–(14) *when the coefficient* α *in the Beavers–Joseph* (12) *condition is small enough.*

Proof Based on the Lemmas 1, 2 and 3, there exists a unique weak solution $\underline{u}$ by the Lax-Milgram Lemma. Then the assertion about p_s is clear, by following the derivations in the deterministic scenario [56,79,96]. $\qquad\square$

4 Numerical Solution for the Stochastic Coupled Problem

Since the moments are the characteristic functions of the stochastic solution, the object is to design a numerical method to calculate the moments of the stochastic solution. The main difficulty in this design is how to represent the stochastic solution by a discrete form in the probability space and the physical space. For the discrete form in the probability space, we choose the ensemble representations in sampling methods, e.g., Monte Carlo (MC) method in this paper. But the total computational cost of the classical single-level Monte Carlo (SLMC) method is very expensive. Then the multilevel Monte Carlo (MLMC) method is adopted to reduce the total computational cost in the probability space. For the discretization in the physical space, the finite element method (FEM) is utilized. Furthermore the multigrid (MG) method is used to reduce the computational cost in the physical space. Finally, the multigrid multilevel Monte Carlo (MGMLMC) method is developed to reduce the computational cost both in the probability space and the physical space.

4.1 Realizations of the Random Hydraulic Conductivity

The realizations of the random hydraulic conductivity $\mathbb{K}(\omega, x)$ in a discrete form on the spatial domain $\bar{D}_m$ and the random field Ω are the basis of the numerical method. We adopt the grid based method in [59] to represent the random field at the discrete points $x_1, \ldots, x_M \in \bar{D}_m$.

For simplification, we assume $\mathbb{K}(\omega, x) = \text{diag}\big(K_{11}(\omega, x), \ldots, K_{dd}(\omega, x)\big), \omega \in \Omega, x \in \bar{D}_m, d = 2, 3$ is a diagonal matrix. The process to generate the realizations of $K(\omega, x) = K_{11}(\omega, x)$ is displayed as follows, which is the same as the processes to generate the realizations of $K_{ii}(\omega, x), i = 2, 3$.

Up to a multiplicative constant, $K(\omega, x)$ is assumed to be a log-normal distribution to meet the positivity of $K(\omega, x)$ in the physical sense, i.e.,

$$K(\omega, x) = e^{Z(\omega, x)}, \quad \omega \in \Omega, \ x \in \bar{D}_m, \tag{26}$$

where $Z(\omega, x)$ is a mean zero Gaussian random field on $\bar{D}_m$, with the continuous covariance function $r(x, y), x, y \in \bar{D}_m$, i.e.,

$$\mathbb{E}[Z(\omega, x)] = 0, \quad \forall x \in \bar{D}_m, \tag{27}$$

$$\mathbb{E}[Z(\omega, x), Z(\omega, y)] = r(x, y), \quad \forall x, y \in \bar{D}_m. \tag{28}$$

For $x_i \in \bar{D}_m, i = 1, 2, \ldots, M$, the vector $\mathbf{x} = (x_1, x_2, \ldots, x_M)^\top$ represents all the discrete spatial points in $\bar{D}_m$, on which $Z(\omega, x)$ is approximated by its discrete form $Z(\omega, \mathbf{x}) = (Z_1, Z_2, \ldots, Z_M)^\top, Z_i = Z(\omega, x_i)$.

Then the discrete form of the covariance function r(x, y) at the discrete points $\mathbf{x}$ is given by a $M \times M$ positive definite matrix R as

$$R = \mathbb{E}\big[Z(\omega, \mathbf{x}), Z(\omega, \mathbf{x})^\top\big] = \big(r(x_i, x_j)\big)_{i,j=1}^M. \tag{29}$$

Let Θ be the Cholesky factorization of R as $R = \Theta\Theta^\top$. Then the random field $Z(\omega, \mathbf{x})$ at the discrete points $\mathbf{x}$ is given by

$$Z(\omega, \mathbf{x}) = \Theta Y(\omega), \tag{30}$$

where $Y(\omega) := (Y_1(\omega), Y_2(\omega), \ldots, Y_M(\omega))^\top$ is a $M \times 1$ vector of independent identically distributed standard Gaussian random variables. And the discrete form $Z(\omega, \mathbf{x})$ is a mean zero Gaussian random vector with the covariance R, since $Z(\omega, \mathbf{x})$ satisfies

$$\mathbb{E}[Z(\omega, \mathbf{x})] = \mathbb{E}[\Theta Y] = \Theta\mathbb{E}[Y] = \mathbf{0},$$

$$\mathbb{E}[Z(\omega, \mathbf{x}), Z(\omega, \mathbf{x})^\top] = \mathbb{E}[(\Theta Y)(\Theta Y)^\top] = \Theta\mathbb{E}[YY^\top]\Theta^\top = \Theta\Theta^\top = R.$$

It is obvious that the approximation $Z(\omega, \mathbf{x})$ at the discrete points $\mathbf{x}$ will be more accurate when the number of the discrete points $x_1, \ldots, x_M$ becomes larger and the discrete form of the covariance function r with matrix R is more accurate. Then the realizations of $K(\omega^i, \mathbf{x}), i = 1, 2, \ldots, N^{\text{MC}}, N^{\text{MC}} \in \mathbb{Z}$ at the discrete points $\mathbf{x}$ are generated as follows:

$$K(\omega^i, \mathbf{x}) = e^{Z(\omega^i, \mathbf{x})}, \quad Z(\omega^i, \mathbf{x}) = \Theta Y(\omega^i),$$

where $Y(\omega^i), i = 1, 2, \ldots, N^{\text{MC}}$ are the realizations of $Y(\omega)$.

Since the realizations $Y(\omega^i)$ of the standard Gaussian random vector Y are bounded, then the the realizations $Z(\omega^i, \mathbf{x})$ are bounded. Hence the realizations of $K(\omega^i, \mathbf{x})$ are bounded and positive, which satisfy (25). Some samples of the realizations of the random hydraulic conductivity K will be displayed in the numerical experiment section.

4.2 Monte Carlo Methods

The Monte Carlo method [99] is a classical method to calculate the numerical approximation of moments. In this paper, we only investigate the process to generate the expected value of ϕ_m, $\mathbf{u}_s$ and p_s, which is easy to be used for the high order of moments.

For simplification, the symbol $Q(\omega, x)$ is used to substitute the exact solution of the variable ϕ_m, $\mathbf{u}_s$ or p_s. Then, let $Q_\ell(\omega, x)$ denote the finite element approximation of $Q(\omega, x)$ on the quasi-uniform triangulation mesh $\mathcal{T}_\ell$ with the mesh size h_ℓ, and $Q_\ell^i(x)$ denote the realization of $Q_\ell(\omega, x)$ with the sample $\mathbb{K}(\omega^i, x)$. Then the approximation $\hat{Q}_\ell^{\mathrm{SL}}(x)$ of the expected value of $Q(\omega, x)$ by SLMC method with N_ℓ^{SL} samples $\{\mathbb{K}(\omega^i, x)\}_{i=1}^{N_\ell^{\mathrm{SL}}}$ is given as:

$$\hat{Q}_\ell^{\mathrm{SL}}(x) = \frac{1}{N_\ell^{\mathrm{SL}}} \sum_{i=1}^{N_\ell^{\mathrm{SL}}} Q_\ell^i(x). \tag{31}$$

When no ambiguity arises, we may omit x in $Q_\ell(x)$, $Q_\ell^i(x)$ and $\hat{Q}_\ell(x)$ for convenience.

The mean squared error of the SLMC method is:

$$\begin{aligned}
MSE(\hat{Q}_\ell^{\mathrm{SL}}) &= \mathbb{E}[(\hat{Q}_\ell^{\mathrm{SL}} - \mathbb{E}[Q])^2] \\
&= \mathbb{E}[(\hat{Q}_\ell^{\mathrm{SL}} - \mathbb{E}[Q_\ell] + \mathbb{E}[Q_\ell] - \mathbb{E}[Q])^2] \\
&\leq 2\mathbb{E}[(\hat{Q}_\ell^{\mathrm{SL}} - \mathbb{E}[Q_\ell])^2] + 2\mathbb{E}[(\mathbb{E}[Q_\ell] - \mathbb{E}[Q])^2] \\
&= \frac{2\mathbb{V}[Q_\ell]}{N_\ell^{\mathrm{SL}}} + 2(\mathbb{E}[Q_\ell] - \mathbb{E}[Q])^2.
\end{aligned} \tag{32}$$

Then the error of SLMC method with a given norm $\|\cdot\|$ is bounded as

$$\|MSE(\hat{Q}_\ell^{\mathrm{SL}})\| \leq \frac{2\|\mathbb{V}[Q_\ell]\|}{N_\ell^{\mathrm{SL}}} + 2\|(\mathbb{E}[Q_\ell] - \mathbb{E}[Q])^2\|, \tag{33}$$

i.e., the accuracy of SLMC method is based on the sampling error and the FEM error.

4.3 Multilevel Monte Carlo Method

The total computational cost T_c^{SL} of single-level Monte Carlo is

$$T_c^{\mathrm{SL}} = N_\ell^{\mathrm{SL}} C_\ell, \tag{34}$$

where C_ℓ is the computational cost of one sample with mesh size h_ℓ. T_c^{SL} would be very high when N_ℓ^{SL} and C_ℓ are both very large. By the accuracy formulation (33) of SLMC method, the sampling error and the FEM error should be both small enough, if a small mean squared error is required. Thus N_ℓ^{SL} should be larger while the mesh size h_ℓ becomes smaller. On the other hand, C_ℓ increases exponentially as the mesh size h_ℓ becomes smaller. Thus the total computational cost increases very fast as mesh size h_ℓ become smaller. An efficient algorithm is needed to reduce the total computational cost. Hence we adopt the multilevel Monte Carlo (MLMC) method.

By the linearity of the expectation operator

$$\mathbb{E}[Q_L] = \mathbb{E}[Q_0] + \sum_{\ell=1}^{L} \left(\mathbb{E}[Q_\ell] - \mathbb{E}[Q_{\ell-1}] \right) = \mathbb{E}[Q_0] + \sum_{\ell=1}^{L} \mathbb{E}[Q_\ell - Q_{\ell-1}], \tag{35}$$

we can use the hierarchical meshes to construct the MLMC method to generate the expect value of Q. Let $\{\mathcal{T}_\ell\}_{\ell=0}^L$ be a sequence of quasi-uniform triangulation meshes with the mesh sizes $\{h_\ell\}_{\ell=0}^L$. These mesh sizes satisfy $h_\ell = h_0 c_h^{-\ell}$, $\ell = 0, 1, 2, \ldots, L$. And $\{N_\ell^{\mathrm{ML}}\}_{\ell=0}^L$ are the numbers of samples with the mesh sizes $\{h_\ell\}_{\ell=0}^L$. Then, from (35) the approximation $\hat{Q}_L^{\mathrm{ML}}$ of the expected value by the MLMC method is given by:

$$\hat{Q}_L^{\mathrm{ML}} = \frac{1}{N_0^{\mathrm{ML}}} \sum_{i=1}^{N_0^{\mathrm{ML}}} Q_0^i + \sum_{\ell=1}^L \frac{1}{N_\ell^{\mathrm{ML}}} \sum_{i=1}^{N_\ell^{\mathrm{ML}}} (Q_\ell^i - Q_{\ell-1}^i). \tag{36}$$

In Sect. 4.4 this formula will be used to compute the expected value in Algorithm 2. When computing the results for step L, one only needs to solve for Q_L^i since all the Q_ℓ^i ($\ell = 0, \ldots, L-1$) were already solved and saved in the previous steps.

Based on the derivation of the mean squared error of the SLCM method in formula (32), the corresponding mean squared error of the MLCM method with norm $\|\cdot\|$ is given by

$$\begin{aligned}
\|MSE(\hat{Q}_L^{\mathrm{ML}})\| &= \|\mathbb{E}[(\hat{Q}_L^{\mathrm{ML}} - \mathbb{E}[Q])^2]\| \\
&\leq 2\frac{\|\mathbb{V}[Q_0]\|}{N_0^{\mathrm{ML}}} + 2\sum_{\ell=1}^L \frac{\|\mathbb{V}[Q_\ell - Q_{\ell-1}]\|}{N_\ell^{\mathrm{ML}}} \\
&\quad + 2\|(\mathbb{E}[Q_L] - \mathbb{E}[Q])^2\|.
\end{aligned} \tag{37}$$

For simplicity, let $Q_{-1} = 0$, $h_{-1} = 0$, $v_\ell = \|\mathbb{V}[Q_\ell - Q_{\ell-1}]\|$, $\ell = 0, 1, 2, \ldots, L$. Then the mean squared error is rewritten as

$$\|MSE(\hat{Q}_L^{\mathrm{ML}})\| \leq 2\sum_{\ell=0}^L \frac{v_\ell}{N_\ell^{\mathrm{ML}}} + 2\|(\mathbb{E}[Q_L] - \mathbb{E}[Q])^2\|. \tag{38}$$

And the total computational cost of MLMC method is given as:

$$T_c^{\mathrm{ML}} = \sum_{\ell=0}^L N_\ell^{\mathrm{ML}} C_\ell. \tag{39}$$

By the mean squared error of SLMC method (33) and MLMC method (38), the accuracy of approximation of expected value is based on two parts, i.e., the sampling error and FEM error. To guarantee the accuracy of the numerical approximations, both the sampling error and FEM error should be smaller than the required error. We substitute the sampling errors in SLMC method and MLMC method by:

$$e_L^{\mathrm{SL}} = \frac{\|\mathbb{V}[Q_L]\|}{N_L^{\mathrm{SL}}}, \quad \text{and} \quad e_L^{\mathrm{ML}} = \sum_{\ell=0}^L \frac{v_\ell}{N_\ell^{\mathrm{ML}}}. \tag{40}$$

For guaranteeing the accuracy of MLMC method to be the same as that of SLMC method, the following relationship between two sampling errors should be ensured

$$e_L^{\mathrm{ML}} \leq e_L^{\mathrm{SL}}, \quad \text{i.e.,} \quad \frac{v_0}{N_0^{\mathrm{ML}}} + \frac{v_1}{N_1^{\mathrm{ML}}} + \cdots + \frac{v_L}{N_L^{\mathrm{ML}}} \leq \frac{\|\mathbb{V}[Q_L]\|}{N_L^{\mathrm{SL}}}. \tag{41}$$

Then we show our strategy to generate the key parameters for MLMC method: the total number of levels (L), and the number of samples at every level $\left(\{N_\ell^{\mathrm{ML}}\}_{\ell=0}^L\right)$.

We take by $L = \log_2(h_0/h_L)$, where the smallest mesh size h_L is determined by the accuracy of FEM required by the practical problem, and the largest mesh size h_0 is constrained by the size of the physical area.

The guideline in designing the number of samples at every level is to minimize the computational cost under the given sampling error. Then, from (39) we introduce the optimization problem as follow:

$$
\begin{cases}
\text{Minimize } T_c^{ML} = N_0^{ML} C_0 + N_1^{ML} C_1 + \cdots + N_L^{ML} C_L, \\
\text{subject to } \frac{v_0}{N_0^{ML}} + \frac{v_1}{N_1^{ML}} + \cdots + \frac{v_L}{N_L^{ML}} = e_L^{ML}.
\end{cases}
\tag{42}
$$

This optimization problem is solved by the method of Lagrangian multipliers:

$$
\begin{aligned}
\mathcal{L} =& N_0^{ML} C_0 + N_1^{ML} C_1 + \cdots + N_L^{ML} C_L \\
& + \lambda \left(\frac{v_0}{N_0^{ML}} + \frac{v_1}{N_1^{ML}} + \cdots + \frac{v_L}{N_L^{ML}} - e_L^{ML} \right).
\end{aligned}
\tag{43}
$$

Then the equations for $\{N_\ell^{ML}\}_{\ell=0}^{L}$ are

$$
\begin{cases}
\frac{\partial \mathcal{L}}{\partial N_\ell^{ML}} = C_\ell - \lambda \frac{v_\ell}{(N_\ell^{ML})^2} = 0, \ for \ \ell = 0, 1, \ldots, L, \\
\frac{\partial \mathcal{L}}{\partial \lambda} = \frac{v_0}{N_0^{ML}} + \frac{v_1}{N_1^{ML}} + \cdots + \frac{v_L}{N_L^{ML}} - e_L^{ML} = 0.
\end{cases}
\tag{44}
$$

Then the number of samples at every level is

$$
N_\ell^{ML} = \sqrt{\frac{v_\ell}{C_\ell}} \left(\frac{\sqrt{v_0 C_0} + \sqrt{v_1 C_1} + \cdots + \sqrt{v_L C_L}}{e_L^{ML}} \right),
\tag{45}
$$

and the optimal computational cost is

$$
T_c^{opt} = T_c^{ML} = \frac{\left(\sqrt{v_0 C_0} + \sqrt{v_0 C_0} + \cdots + \sqrt{v_L C_L} \right)^2}{e_L^{ML}}.
\tag{46}
$$

In conclusion, based on this strategy, we can obtain the number of samples at every level while the parameters e_L^{ML}, $\{C_\ell\}_{\ell=0}^{L}$, $\{v_\ell\}_{\ell=0}^{L}$ are given.

Furthermore, we assume $v_\ell = \mathcal{O}(h_\ell^\beta)$ by the virtue of experience, and $C_\ell = \mathcal{O}(h_\ell^{-\gamma})$ with the reason that the amount of calculated information increases exponentially while the mesh size becomes smaller. Then with $h_\ell = h_0 2^{-\ell}$, $\ell = 0, 1, \ldots, L$, and (45), for any $j > i$, the relationship between the numbers of samples at two levels is given as

$$
\frac{N_j^{ML}}{N_i^{ML}} = \sqrt{\frac{C_i}{v_i} \cdot \frac{v_j}{C_j}} = \sqrt{\mathcal{O}\left(\left(\frac{h_j}{h_i} \right)^{\beta+\gamma} \right)} = \mathcal{O}\left(2^{-\frac{(j-i)(\beta+\gamma)}{2}} \right) < 1.
\tag{47}
$$

Thus the number of samples becomes smaller while mesh size becomes smaller. The decrease of N_ℓ^{ML} is the reason why the MLMC method can reduce the total computational cost.

Since the computational cost of every sample with the mesh size h_0 is low, v_0 is easy to calculate by Monte Carlo method with low computational cost. Then v_ℓ, $\ell = 1, \ldots, L$, can be given by $v_\ell = \mathcal{O}(h_\ell^\beta)$ with the corresponding parameter β. Thus how to determine parameter β is a key problem for the MLMC method. In this paper, for the Stokes–Darcy interface problem with Beavers–Joseph condition, we develop a strategy for calculating the parameter β in the Sect. 5.2.

4.4 Combine the Multigrid Method with the Multilevel Monte Carlo Method

The total computational cost is determined by the number of samples and the computational cost of every sample. Since we have reduced the total computational cost in probability space with the MLMC method by reducing the number of samples, it is a heuristic problem whether we could reduce computational cost of every sample to save the total computational cost in physical space. Inspired by the hierarchical meshes used in the MLMC method, we adopt the multigrid (MG) method to reduce the computational cost of every sample in physical space.

In the physical space, the finite element method (FEM) is chosen to construct the discrete form of weak formulation (16) under the given samples of hydraulic conductivity. We adopt the quadratic element in the porous media domain, and the Taylor-Hood element in the conduit domain. Then for every given sample of hydraulic conductivity $\mathbb{K}(\omega, x)$, the weak formulation (16) is discretized into the following matrix-vector form

$$\mathbf{L}\mathbf{x} = \mathbf{b}, \quad \mathbf{L} = \begin{pmatrix} A_m & B_1 & 0 \\ B_2 & A_s & B_p' \\ 0 & B_p & 0 \end{pmatrix}, \quad \mathbf{x} = \begin{pmatrix} \phi_m \\ \mathbf{u}_s \\ p \end{pmatrix}, \quad \mathbf{b} = \begin{pmatrix} b_m \\ \mathbf{b}_s \\ 0 \end{pmatrix}. \tag{48}$$

where A_m is the matrix corresponding to the discretization of $g \int_{D_m} (\mathbb{K}\nabla\phi_m) \cdot \nabla\psi_m dx$, B_1 is the matrix corresponding to the discretization of $-g \int_{\Gamma_I} (\mathbf{u}_s \cdot \mathbf{n}_s)\psi_m d\Gamma_I$, B_2 is the matrix corresponding to the discretization of $\int_{\Gamma_I} g\phi_m \mathbf{v}_s \cdot \mathbf{n}_s d\Gamma_I + \int_{\Gamma_I} \frac{\alpha\nu\sqrt{d}}{\sqrt{\text{trace}(\Pi)}} P_\tau (\mathbb{K}\nabla\phi_m) \cdot \mathbf{v}_s d\Gamma_I$, A_s is the matrix corresponding to the discretization of $\int_{D_s} 2\nu\mathbb{D}(\mathbf{u}_s) : \mathbb{D}(\mathbf{v}_s) dx + \int_{\Gamma_I} \frac{\alpha\nu\sqrt{d}}{\sqrt{\text{trace}(\Pi)}} P_\tau (\mathbf{u}_s) \cdot \mathbf{v}_s d\Gamma_I$, B_p' is the matrix corresponding to the discretization of $\int_{D_s} p_s \nabla \cdot \mathbf{v}_s dx$, b_m is the vector corresponding to the discretization of $g \int_{D_m} f_m \psi_m dx$, and $\mathbf{b}_s$ is the vector corresponding to the discretization of $\int_{D_s} \mathbf{f}_s \cdot \mathbf{v}_s dx + \int_{\Gamma_I} gz\mathbf{v}_s \cdot \mathbf{n}_s d\Gamma_I$.

Inspired by the multigrid method for Stokes equations, we adopt the efficient least square commutator distributive Gauss-Seidel (LSC-DGS) relaxation [29,113] in this paper. The right-side operator $\mathbf{M}$ is given as:

$$\mathbf{M} = \begin{pmatrix} I & 0 & 0 \\ 0 & I & B_p' \\ 0 & 0 & -(B_p B_p')^{-1} B_p A_s B_p' \end{pmatrix}. \tag{49}$$

Multiplying $\mathbf{L}$ with $\mathbf{M}$ yields

$$\mathbf{L}\mathbf{M} = \begin{pmatrix} A_m & B_1 & B_1 B_p' \\ B_2 & A_s & W \\ 0 & B_p & B_p B_p' \end{pmatrix}, \quad \text{with } W = \left(I - B_p'(B_p B_p')^{-1} B_p \right) A_s B_p'.$$

By defining $\mathbf{S} := \mathbf{L}\mathbf{M}$ and $\mathbf{y} := \mathbf{M}^{-1}\mathbf{x}$, the equivalent algebraic equations are given as

$$\mathbf{S}\mathbf{y} = \mathbf{b}. \tag{50}$$

The standard Gauss–Seidel method is proposed to solve the equivalent algebraic equations (50). And the following $\mathcal{V}$-cycle multigrid method is applied to reduce the computational cost in physical space. As in the MLMC method, the hierarchical quasi-uniform triangulation meshes are $\mathcal{T}_\ell$ with the mesh sizes $h_\ell = h_0 c_h^{-\ell}$, $\ell = 0, 1, 2, \ldots, L$. Then the $\mathcal{V}$-cycle multigrid method on the mesh $\mathcal{T}_\ell$ with the mesh size h_ℓ is given as [108]:

Algorithm 1 $\mathbf{y}^{new} \leftarrow \mathcal{V} - cycle(\mathbf{S}, \mathbf{b}, \ell)$

(1) *Relax λ_1 times on the fine mesh $h = h_\ell$ with the initial guess $\mathbf{y}$ to reach $\mathbf{y}^h$.*

(2) *Obtain the residual on the fine mesh as*

$$r^h = \mathbf{b} - \mathbf{S}\mathbf{y}^h,$$

and restrict the residual from the fine mesh h to the coarse mesh $H = h_{\ell-1}$ by $r^H = \mathcal{R}_h^H r^h$, where $\mathcal{R}_h^H$ is the restriction matrix.

(3) *Solve the corrected error from the residual equation on the coarse mesh H:*

   – *If $\ell = 1$, use a direct or fast iterative method to solve $\mathbf{S}^H e^H = r^H$;*
   – *If $\ell > 1$, use the ℓ-grid method to solve $\mathbf{S}^H e^H = r^H$ from a zero initial guess on the mesh $\mathcal{T}_{\ell-1}$ by $e^H \leftarrow \mathcal{V} - cycle(\mathbf{S}^H, r^H, \ell - 1)$;*

   where $\mathbf{S}^H$ is the approximation of $\mathbf{S}$ on the coarse mesh.

(4) *Prolongate the corrected error form coarse mesh H to the fine mesh h by $e^h = \mathcal{I}_H^h e^H$, where $\mathcal{I}_H^h$ is the interpolation matrix. And correct the approximation by*

$$\mathbf{y}^{new} = \mathbf{y}^h + e^h.$$

(5) *Relax λ_2 times on the fine mesh h with the initial guess $\mathbf{y}^{new}$.*

One can also replace the $\mathcal{V}$-cycle by $\mathcal{W}$-cycle or $\mathcal{F}$-cycle [16,17,29,90,106,113]. Furthermore, the solutions calculated on the coarse mesh in the MLMC method could be used as the initial guess on the fine mesh in the MG method to further reduce the computational cost. Then the following multigird multilevel Monte Carlo (MGMLMC) method is developed to reduce the computational cost in both the probability space and the physical space.

Algorithm 2 *multigrid multilevel Monte Carlo method*

(1) *On the mesh grid $\mathcal{T}_0$ with the mesh size h_0, for the 1st to the N_0^{ML} sample of hydraulic conductivity $\mathbb{K}(\omega, x)$, solve the numerical approximations Q_0^i by standard Gauss-Seidel with the initial guess $\mathbf{0}$, $i = 1, 2, \ldots, N_0^{ML}$;*

(2) *For $\ell = 1, 2, \ldots, L$, consider the mesh grid $\mathcal{T}_\ell$ with the mesh size h_ℓ. For the 1st to the N_ℓ^{ML} sample of hydraulic conductivity $\mathbb{K}(\omega, x)$, solve the numerical approximations Q_ℓ^i by $\mathcal{V}$-cycle $(\ell + 1)$-grid method (Algorithm 1) with the initial guess $\mathcal{I}_H^h Q_{\ell-1}^i$, $i = 1, 2, \ldots, N_\ell^{ML}$, where $h = h_\ell$ and $H = h_{\ell-1}$;*

(3) *Based on the numerical solutions Q_ℓ^i gained in the above two steps on every mesh grid $\mathcal{T}_\ell$ with each hydraulic conductivity sample $\mathbb{K}(\omega^i, x)$, $i = 1, 2, \ldots, N_\ell^{ML}$, $\ell = 0, 1, \ldots, L$, the approximation $\hat{Q}_L^{ML}$ of the expected value by the MGMLMC method is computed (36).*

4.5 Computational Cost of SLMC Method and MGMLMC Method

Based on the conclusions in the Sects. 4.2 and 4.3, we gain the relationships between the sampling error and the FEM error in the SLMC method and the MLMC method. Notice that, the sampling error is determined by the number of samples, and the FEM error is determined by the mesh size of the quasi-uniform triangulation mesh. Then we can gain the relationships between the number of samples and the mesh size in the SLMC method and the MLMC method. Furthermore, the mesh size also determines the computational cost of one sample. Then we can give an estimate of the total computational costs of the MLMC (or MGMLMC) method and the SLMC method, with the given mesh size.

First, the numerical error is estimated as follow:

Proposition 1 *With the assumption* (25), *the solutions of problem* (16) *satisfy the following discrete error estimate*

$$\|\underline{u} - \underline{u}_\ell\|_{X^0} + \|p_s - p_{\ell,s}\|_{\mathcal{L}^2(D_s)} \le C h_\ell \Big(\|\underline{u}\|_{X^1} + \|p_s\|_{\mathcal{L}^2(D_s)} \Big), \tag{51}$$

where h_ℓ is the mesh size of the given quasi-uniform triangulation mesh $\mathcal{T}_\ell$.

Proof Based on the analysis in [23,24,79], we have

$$\|\mathbf{u}_s(\omega, \cdot) - \mathbf{u}_{\ell,s}(\omega, \cdot)\|_{\mathbf{H}^0(D_s)} + \|\phi_m(\omega, \cdot) - \phi_{\ell,m}(\omega, \cdot)\|_{H^0(D_m)}$$
$$+ \|p_s(\omega, \cdot) - p_{\ell,s}(\omega, \cdot)\|_{L^2(D_s)}$$
$$\le C h_\ell \Big(\|\mathbf{u}_s(\omega, \cdot)\|_{\mathbf{H}^1(D_s)} + \|\phi_m(\omega, \cdot)\|_{H^1(D_m)}$$
$$+ \|p_s(\omega, \cdot)\|_{L^2(D_s)} \Big), \text{ a.e. } \omega \in \Omega.$$

Then the assertion follows with the above conclusion by the definition of the norm $\|\cdot\|_{X^0}$ in (15). $\qquad\square$

Then the numerical errors of SLMC method and MGMLMC method are bounded by the mesh size h_ℓ and the number of samples N_ℓ.

Lemma 4 *With the assumption* (25), *the error bounds of SLMC method* (31) *and MLMC* (36) *for the problem* (16) *are given as follows*

$$\|\mathbb{E}[\underline{u}] - \hat{\underline{u}}_\ell^{SL}\|_{X^0} + \|\mathbb{E}[p_s] - \hat{p}_{s,\ell}^{SL}\|_{\mathcal{L}^2(D_s)} \le C(\underline{u}, p_s)\left(h_\ell + \frac{1}{\sqrt{N_\ell^{SL}}}\right), \tag{52}$$

$$\|\mathbb{E}[\underline{u}] - \hat{\underline{u}}_L^{ML}\|_{X^0} + \|\mathbb{E}[p_s] - \hat{p}_{s,L}^{ML}\|_{\mathcal{L}^2(D_s)} \le C(\underline{u}, p_s)\left(h_L + \sum_{\ell=0}^{L} \frac{h_\ell}{\sqrt{N_\ell^{ML}}}\right), \tag{53}$$

where C depends on $\underline{u}$ and p_s, h_ℓ is the mesh size of the quasi-uniform triangulation mesh $\mathcal{T}_\ell$, N_ℓ^{SL} is the number of samples with mesh size h_ℓ in SLMC method, N_ℓ^{ML} is the number of samples with mesh size h_ℓ in MLMC method, $\hat{\underline{u}}_\ell^{SL}$, $\hat{p}_{s,\ell}^{SL}$ are the approximations of expect value by SLMC method, and $\hat{\underline{u}}_\ell^{ML}$, $\hat{p}_{s,\ell}^{ML}$ are the approximations of expect value by MLMC method, $\ell = 0, 1, \dots, L$.

Proof For simplification, let the symbol Q substitute the variables ϕ_m, u_s or p_s. And let $\mathcal{L}(V)$ denote the corresponding space of Q. Thus $\mathcal{L}(V)$ may denote $\mathcal{H}^1(D_m)$, $\mathcal{L}^2(D_s)$ or $\mathcal{H}^1(D_s)$, and V may be $H^1(D_m)$, $L^2(D_s)$ or $\mathbf{H}^1(D_s)$, which depends on the choice of Q. Then we analyse the error of the approximation of expect value of ϕ_m, u_s or p_s by analysing $\mathbb{E}[Q] - \hat{Q}_\ell^{SL}$ with the norm $\|\cdot\|_{\mathcal{L}(V)}$ as follow:

$$\|\mathbb{E}[Q] - \hat{Q}_\ell^{SL}\|_{\mathcal{L}(V)} = \|\mathbb{E}[Q] - \mathbb{E}[Q_\ell] + \mathbb{E}[Q_\ell] - \hat{Q}_\ell^{SL}\|_{\mathcal{L}(V)}$$
$$\le \|\mathbb{E}[Q] - \mathbb{E}[Q_\ell]\|_{\mathcal{L}(V)} + \|\mathbb{E}[Q_\ell] - \hat{Q}_\ell^{SL}\|_{\mathcal{L}(V)}. \tag{54}$$

For $\|\mathbb{E}[Q] - \mathbb{E}[Q_\ell]\|_{\mathcal{L}(V)}$, we have

$$\|\mathbb{E}[Q] - \mathbb{E}[Q_\ell]\|_{\mathcal{L}(V)}^2 = \|\mathbb{E}[Q - Q_\ell]\|_{\mathcal{L}(V)}^2 = \mathbb{E}\big[\|\mathbb{E}[Q - Q_\ell]\|_V^2\big]$$
$$= \|\mathbb{E}[Q - Q_\ell]\|_V^2 \le \mathbb{E}[\|Q - Q_\ell\|_V^2] \tag{55}$$
$$= \|Q - Q_\ell\|_{\mathcal{L}(V)}^2.$$

For $\|\mathbb{E}[Q_\ell] - \hat{Q}_\ell^{\mathrm{SL}}\|_{\mathcal{L}(V)}$, we have

$$
\begin{aligned}
\|\mathbb{E}[Q_\ell] - \hat{Q}_\ell^{\mathrm{SL}}\|_{\mathcal{L}(V)}^2 &= \mathbb{E}\left[\left\|\mathbb{E}[Q_\ell] - \frac{1}{N_\ell^{\mathrm{SL}}}\sum_{i=1}^{N_\ell^{\mathrm{SL}}} Q_\ell^i\right\|_V^2\right] \\
&= \frac{1}{(N_\ell^{\mathrm{SL}})^2}\mathbb{E}\left[\left\|\sum_{i=1}^{N_\ell^{\mathrm{SL}}} \left(\mathbb{E}[Q_\ell] - Q_\ell^i\right)\right\|_V^2\right] \\
&\le \frac{1}{(N_\ell^{\mathrm{SL}})^2}\mathbb{E}\left[\sum_{i=1}^{N_\ell^{\mathrm{SL}}} \left\|\mathbb{E}[Q_\ell] - Q_\ell^i\right\|_V^2\right] \\
&= \frac{1}{N_\ell^{\mathrm{SL}}}\mathbb{E}\left[\|\mathbb{E}[Q_\ell] - Q_\ell\|_V^2\right] \\
&\le \frac{1}{N_\ell^{\mathrm{SL}}}\|Q_\ell\|_{\mathcal{L}(V)}^2.
\end{aligned}
\tag{56}
$$

The last inequality is based on $\mathbb{E}[(\mathbb{E}[Q_\ell] - Q_\ell)^2] = \mathbb{E}[(Q_\ell)^2] - (\mathbb{E}[Q_\ell])^2 \le \mathbb{E}[(Q_\ell)^2]$.

Thus we obtain

$$
\|\mathbb{E}[Q] - \hat{Q}_\ell^{\mathrm{SL}}\|_{\mathcal{L}(V)} \le (N_\ell^{\mathrm{SL}})^{-1/2}\|Q_\ell\|_{\mathcal{L}(V)} + \|Q - Q_\ell\|_{\mathcal{L}(V)}.
\tag{57}
$$

Then by the Proposition 1, we have

$$
\begin{aligned}
&\|\mathbb{E}[\underline{u}] - \hat{\underline{u}}_\ell^{\mathrm{SL}}\|_{X^0} + \|\mathbb{E}[p_s] - \hat{p}_{s,\ell}^{\mathrm{SL}}\|_{\mathcal{L}^2(D_s)} \\
&\le (N_\ell^{\mathrm{SL}})^{-1/2}\|\underline{u}_\ell\|_{X^0} + \|\underline{u} - \underline{u}_\ell\|_{X^0} \\
&\quad + (N_\ell^{\mathrm{SL}})^{-1/2}\|p_{s,\ell}\|_{\mathcal{L}^2(D_s)} + \|p_s - p_{s,\ell}\|_{\mathcal{L}^2(D_s)} \\
&\le C\left(h_\ell + (N_\ell^{\mathrm{SL}})^{-1/2}\right)\left(\|\underline{u}\|_{X^0} + \|\underline{u}\|_{X^1} + \|p_s\|_{\mathcal{L}^2(D_s)}\right) \\
&= C(\underline{u}, p_s)\left(h_\ell + (N_\ell^{\mathrm{SL}})^{-1/2}\right).
\end{aligned}
$$

where $C(\underline{u}, p_s)$ depends on $\|\underline{u}\|_{X^0}$, $\|\underline{u}\|_{X^1}$ and $\|p_s\|_{\mathcal{L}^2(D_s)}$.

Because the idea to prove the assertion of the MLMC method is the same as that in the proof of the assertion of the SLMC method, we omit the corresponding proof. $\qquad\square$

By equilibrating the sampling error in probability space and the FEM error in physical space, and the conclusions in Lemma 4, we have the following two conclusions:

$$
(e_\ell^{\mathrm{SL}})^{1/2} = \mathcal{O}\left((N_\ell^{\mathrm{SL}})^{-1/2}\right) = \mathcal{O}(h_\ell),
\tag{58}
$$

$$
(e_L^{\mathrm{ML}})^{1/2} = \mathcal{O}\left(\sum_{\ell=0}^{L} h_\ell (N_\ell^{\mathrm{ML}})^{-1/2}\right) = \mathcal{O}(h_L).
\tag{59}
$$

The formula (58) is the relationship between the numbers of samples N_ℓ^{SL} and the mesh sizes h_ℓ in the SLMC method, which is based on the conclusion (52). And the formula (59) is the relationship between the numbers of samples $\{N_\ell^{\mathrm{ML}}\}_{\ell=0}^{L}$ and the mesh sizes $\{h_\ell\}_{\ell=0}^{L}$ in the MLMC method, which is based on the conclusion (53).

In the SLMC method, by (58), it is easy to see that the number of samples N_L^{SL} on the finest mesh is determined by the mesh size h_L, then the computational cost can be calculated. In the MLMC method, the number of samples $\{N_\ell^{\mathrm{ML}}\}_{\ell=0}^{L}$ on every level is determined by the

formula (45). Since the sampling error is bounded by the formula (59), then the computational cost can also be calculated.

Theorem 2 *With the assumption* (25), *for the problem* (16), *if we choose the SLMC method* (31) *on the triangulation mesh* $\mathcal{T}_L$ *with the mesh size* h_L, *or the MGMLMC method Algorithm 2 on the hierarchical quasi-uniform triangulation meshes* $\{\mathcal{T}_\ell\}_{\ell=0}^L$ *with mesh sizes* $h_\ell = h_0 2^{-\ell}$, $\ell = 0, 1, \ldots, L$ *to solve the approximations of expect value, we can evaluate the computational cost as follows:*

$$T_c^{SL} = \mathcal{O}\left(M_L^{2+\frac{2}{d}}\right), \tag{60}$$

$$T_c^{MGML} = \mathcal{O}\left(M_L^{1+\frac{2-\beta}{d}} \log(M_L) 2^{\frac{\beta L}{2}+d-dL}\right), \tag{61}$$

where M_L *is the amount of calculated information for one sample on the mesh* $\mathcal{T}_L$ *with the mesh size* h_L, d *is the dimension of the physical space, and* β *is the decrease rate of the variance. Furthermore, the ratio of the computational cost of the SLMC method and the MGMLMC method is given as*

$$T_c^{SL}/T_c^{MGML} = \mathcal{O}\left(2^{2Ld+\frac{\beta L}{2}-d}/(Ld)\right). \tag{62}$$

Proof Under the assumption $M_\ell = \mathcal{O}\left(h_\ell^{-d}\right)$ and the setting $h_\ell = h_0 2^{-\ell}$, $M_\ell = \mathcal{O}\left(M_L 2^{(\ell-L)d}\right)$ is given. Since the standard Gauss-Seidel method is chosen to solve the algebraic equations (50) in the SLMC method, the computational cost C_ℓ with the mesh size h_ℓ is $C_\ell = \mathcal{O}\left(M_L^2 2^{2(\ell-L)d}\right)$.

For the SLMC method, the number of samples on mesh $\mathcal{T}_L$ with mesh size h_L is $N_L^{\text{SL}} = \mathcal{O}\left(h_L^{-2}\right) = \mathcal{O}\left(M_L^{2/d}\right)$, by the bound of sampling error in (58). Then the computational cost of the SLMC method is $T_c^{SL} = N_L^{\text{SL}} C_L = \mathcal{O}\left(M_L^{2+\frac{2}{d}}\right)$.

For the MGMLMC method, the bound of sampling error is $e_L^{\text{ML}} = \mathcal{O}\left(h_L^2\right) = \mathcal{O}\left(M_L^{-2/d}\right)$ by (59). Since we adopt the $\mathcal{V}$-cycle multigrid methods in this paper, then the computational cost [17,106] on mesh $\mathcal{T}_\ell$ with mesh size h_ℓ is

$$\begin{aligned} C_\ell^{\text{MG}} &= \mathcal{O}\left(M_L 2^{(\ell-L)d}\left(\log(M_L) + d(\ell-L)\log(2)\right)\right) \\ &\leq \mathcal{O}\left(M_L 2^{(\ell-L)d}\log(M_L)\right). \end{aligned} \tag{63}$$
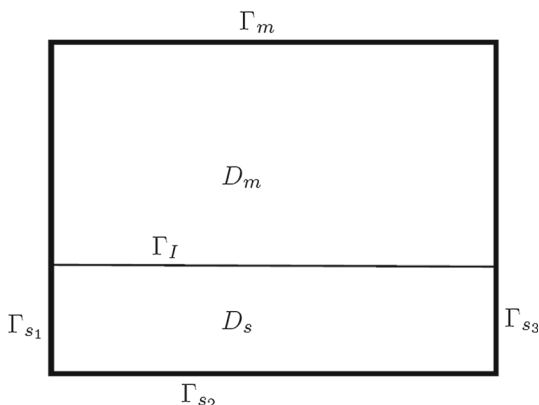
Then by (45), the number of samples at the initial level is

$$\begin{aligned} N_0^{\text{ML}} &= \sqrt{\frac{v_0}{C_0^{\text{MG}}}}\left(\frac{\sqrt{v_0 C_0^{\text{MG}}} + \sqrt{v_1 C_1^{\text{MG}}} + \cdots + \sqrt{v_L C_L^{\text{MG}}}}{e_L^{\text{ML}}}\right) \\ &\leq \mathcal{O}\left(M_L^{\frac{2-\beta}{d}} 2^{\beta L+\frac{d-Ld}{2}}\right). \end{aligned} \tag{64}$$

And by the relationship between the numbers of samples at two different levels (47), the number of samples on mesh $\mathcal{T}_\ell$ with mesh size h_ℓ is

$$N_\ell^{\text{ML}} = N_0^{\text{ML}}\sqrt{\frac{C_0^{\text{MG}}}{v_0} \cdot \frac{v_\ell}{C_\ell^{\text{MG}}}} = \mathcal{O}\left(M_L^{\frac{2-\beta}{d}} 2^{\frac{\beta L-dL+d-d\ell}{2}}\right). \tag{65}$$

Fig. 1 A sketch of two rectangles domain

Then the computational cost of the MGMLMC method is

$$T_c^{\mathrm{MGML}} = \sum_{\ell=0}^{L} N_\ell^{\mathrm{ML}} C_\ell^{\mathrm{MG}} = \mathcal{O}\big(M_L^{1+\frac{2-\beta}{d}} \log(M_L) 2^{\frac{\beta L}{2}+d-dL}\big). \tag{66}$$

By $h_L = h_0 2^{-L}$ and $M_L = \mathcal{O}\big(h_L^{-d}\big)$, we have

$$\frac{T_c^{\mathrm{SL}}}{T_c^{\mathrm{MGML}}} = \frac{\mathcal{O}\big(2^{Ld(2+\frac{2}{d})}\big)}{\mathcal{O}\big(2^{Ld(1+\frac{2-\beta}{d})+\frac{\beta L}{2}+d-dL}Ld\big)} = \mathcal{O}\big(2^{2Ld+\frac{\beta L}{2}-d}/(Ld)\big). \tag{67}$$

$\square$

5 Numerical Experiments

In this section, we use numerical experiments to demonstrate both the features of the MGMLMC method and the theoretical conclusion. The first part is to generate the realizations of random hydraulic conductivity $\mathbb{K}$ by the grid based method. The second part is to determine the key parameter β, which will be used to calculate the $\{N_\ell^{\mathrm{ML}}\}_{\ell=0}^{L}$ in the MLMC method. The last part is to provide the numerical results in detail.

We assume that the domain D_{ms} consists of two rectangles, the upper rectangle is the porous media domain $D_m = (0, 1) \times (0, 0.75)$, and the other rectangle is the conduit domain $D_s = (0, 1) \times (-0.25, 0)$, shown as the Fig. 1. The whole domain $D_{ms} = D_m \cup D_s$ with the interface $\Gamma_I = (0, 1) \times \{0\}$. The boundaries are $\Gamma_m = \{0, 1\} \times (0, 0.75) \cup (0, 1) \times \{0.75\}$ and $\Gamma_s = \Gamma_{s_1} \cup \Gamma_{s_2} \cup \Gamma_{s_3}$, where $\Gamma_{s_1} = \{0\} \times (-0.25, 0)$, $\Gamma_{s_2} = (0, 1) \times \{-0.25\}$, $\Gamma_{s_3} = \{1\} \times (-0.25, 0)$. For simplicity, let $g = 1$, $z = 0$, $\alpha = 1$, $\nu = 1$ and $\mathbb{K}(\omega, x) = e^{Z(\omega,x)}\mathbb{I}$. The covariance function of Z is $r(x, y) = r\big((x_1, x_2), (y_1, y_2)\big) = 0.1 e^{-\frac{|x_1-y_1|}{0.2} - \frac{|x_2-y_2|}{0.2}}$.

5.1 The Realizations of Random Hydraulic Conductivity

Because the diagonal matrix is given as $\mathbb{K}(\omega, x) = e^{Z(\omega,x)}\mathbb{I}$, it is natural to generate the realizations of $K(\omega, x) = e^{Z(\omega,x)}$, and then copy the realizations d times to construct $\mathbb{K}(\omega, x)$. As the hierarchical meshes are used in the MLMC method, the realizations of $K(\omega, x) = e^{Z(\omega,x)}$ could be first generated on the finest mesh by the grid based method. Then the realizations
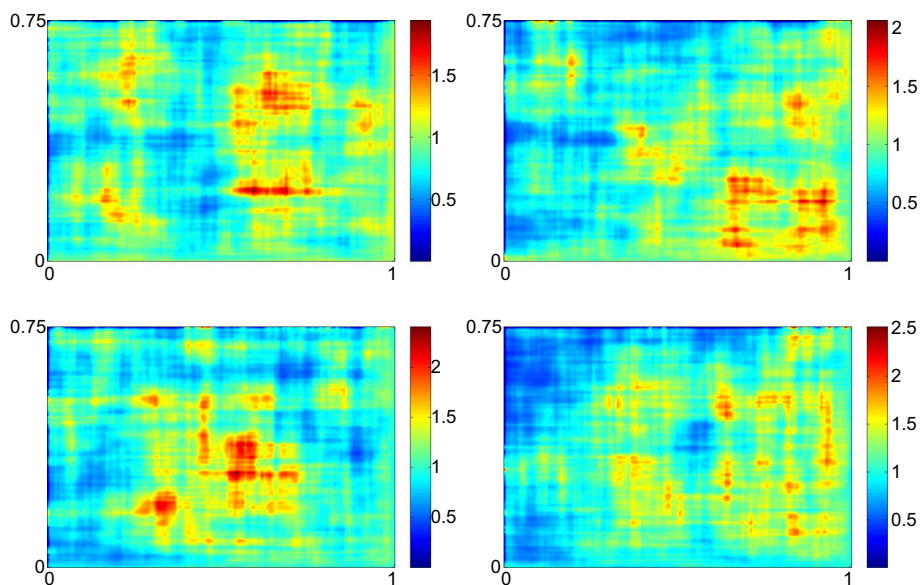
Fig. 2 Four samples of random hydraulic conductivity $K(\omega, x)$

on the coarse mesh can be chosen as a subset of the realizations on the finest mesh. Then the consistency of hydraulic conductivity $K(\omega, x)$ on every mesh could be ensured.

Because the Gauss quadrature is used to compute the integrals in the proposed method, we calculate the value of the approximation of the hydraulic conductivity $K(\omega, x)$ on the Gauss quadrature points by the grid based method. In every triangle of the triangulation mesh $\mathcal{T}_L$, the seven-point Gauss quadrature rule is applied. On the interface, four-point Gauss quadrature rule is applied.

In this experiment, we generate 4000 samples of the hydraulic conductivity $K(\omega, x)$. Four samples of $K(\omega, x)$ are illustrated in Fig. 2, by which the randomness of hydraulic conductivity is exhibited.

5.2 Determination of the Parameter β in MLMC Method

How to determine the parameter β is a key problem in the numerical implementation of MLMC method. If one calculates β from the exact variances $\{v_\ell\}_{\ell=0}^L$, which come from the SLMC method with mesh size $\{h_\ell\}_{\ell=0}^L$, then the computational cost is higher than that of the SLMC method with mesh size h_L. This contradicts the purpose of the MLMC method. In this section, we develop the following practical method to approximate the parameter β without calculating the exact variances $\{v_\ell\}_{\ell=0}^L$.

Since the random hydraulic conductivity is only a parameter in the Darcy domain and on the interface, we assume that the β of the stochastic Darcy problem is an approximation for the β of the stochastic Stokes–Darcy problem with the same random hydraulic conductivity. Compared with the coupled stochastic Stokes–Darcy problem, the computational cost of every sample of the stochastic Darcy problem is much cheaper since the Darcy problem is much simpler. Furthermore, we can also use the multigrid method to reduce the computational cost in generating the approximation of β.
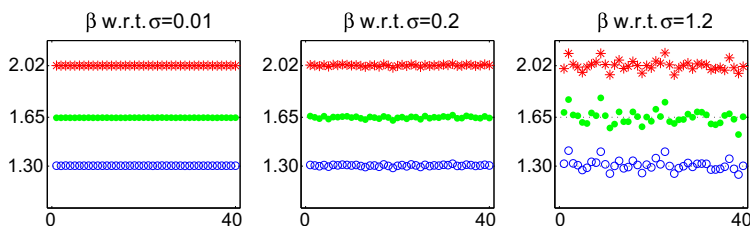
Fig. 3 0, 40 on x-label in every subgraph is the index of 40 samples of f. The red star $*$ are β with $\|\cdot\|_{L_2}$ norm, the green dot $\cdot$ are β with $\|\cdot\|_{L_\infty}$ norm, and the blue circle $\circ$ are β with $\|\cdot\|_{H_1}$ norm

Table 1 Mean values of β with different σ and norm

σ	$\|\cdot\|_{L_2}$	$\|\cdot\|_{L_\infty}$	$\|\cdot\|_{H_1}$
0.02	2.0204	1.6468	1.3030
0.80	2.0216	1.6487	1.3043
1.20	2.0209	1.6511	1.3081

The stochastic Darcy problem is given by

$$
\begin{cases}
-\nabla \cdot \big(\mathbb{K}(\omega, x)\nabla\phi(\omega, x)\big) = f(\omega, x), & (\omega, x) \in \Omega \times D_m, \\
\phi(\omega, x) = 0, & (\omega, x) \in \Omega \times \partial D_m.
\end{cases}
\tag{68}
$$

where $f(\omega, x)$ is a piecewise constant approximation of white noise, i.e.,

$$
f(x) = \sigma \sum_{i=1}^{I} \frac{1}{\sqrt{V_i}} \chi_i(x) X_i(\omega), \quad x \in D_m.
\tag{69}
$$

Here σ is a given constant, V_i is the volume of non-overlapping tessellation $\{D_i\}_{i=1}^{I}$ as $D_m = \cup_{i=1}^{I} D_i$, $\chi_i(x)$ is the indicator function corresponding to D_i, and $\{X_i(\omega)\}_{i=1}^{I}$ is a given set of independent identically distributed standard Gaussian random variables.

Given the σ and $\{X_i(\omega)\}_{i=1}^{I}$ in (69), we could use the SLMC method to calculate $\big\{v_\ell = \|\mathbb{V}[Q_\ell - Q_{\ell-1}]\|\big\}_{\ell=0}^{L}$ with norm $\|\cdot\|$ on the hierarchical quasi-uniform triangulation meshes $\{\mathcal{T}_\ell\}_{\ell=0}^{L}$ with mesh sizes $\{h_\ell\}_{\ell=0}^{L}$. And then the parameter β is determined from the assumption $\big\{v_\ell = \mathcal{O}(h_\ell^\beta)\big\}_{\ell=0}^{L}$. For each $\sigma = 0.02, 0.8, 1.2$, we choose 40 samples of f. For every given σ and one sample of f, three β are calculated with $\|\cdot\|_{L_2}$, $\|\cdot\|_{L_\infty}$ and $\|\cdot\|_{H_1}$ norms. The results of β with each sample of f and the choice of σ are exhibited in Fig. 3. And the mean values of β with 40 samples of f are shown in Table 1. One can see that the mean value of the β changes only in a small range when σ becomes larger. Thus the parameter β is given as 2.02, 1.65, 1.30 w.r.t. $\|\cdot\|_{L_2}$, $\|\cdot\|_{L_\infty}$, $\|\cdot\|_{H_1}$ norms.

In the next section for the results of the stochastic Stokes–Darcy model, it can be seen that the expected accuracy is gained by MGMLMC method with much less samples and computational cost, compared with the SLMC method. Based on the definition and importance of β discussed in Sect. 4.3, this will indicate that the β determined in this section works well for the MGMLMC method of the stochastic Stokes–Darcy model with Beavers–Joesph interface condition.

In addition, compared with the traditional SLMC method, this process in MLMC method will give rise to extra computational cost, whose computational cost should be added to the total computational cost of MLMC method.
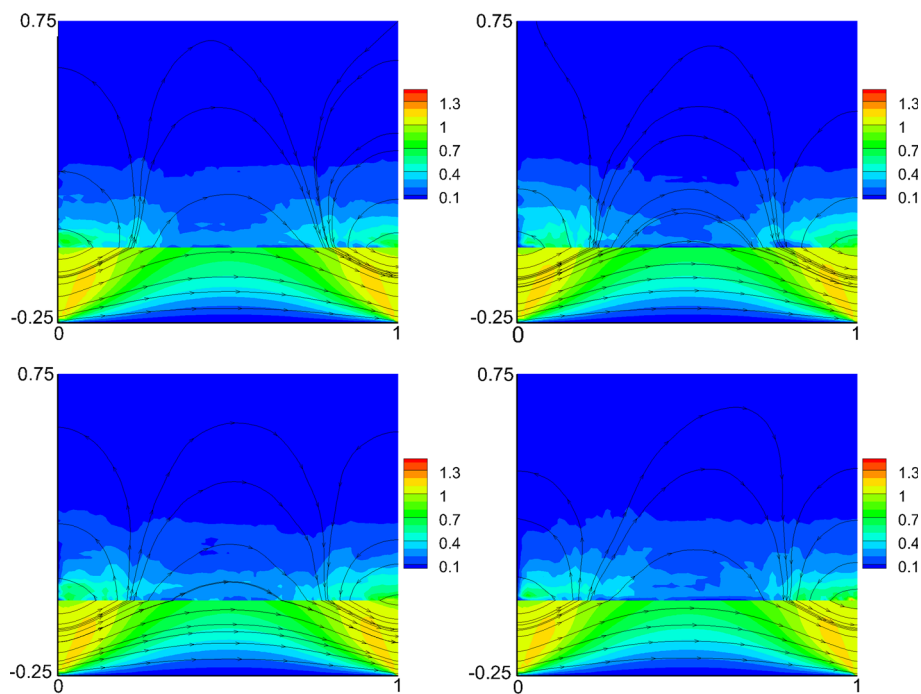
Fig. 4 Four samples of solution and stream lines with $h = 1/64$. Color represents the speed of flow

Table 2 Computational cost with different mesh size	h	1/4	1/8	1/16	1/32
	Cpu time (s)	0.48	1.84	9.64	245.65
	Tic-toc time (s)	0.44	1.43	8.38	240.46

## 5.3 Main Numerical Results

Let $f_m = 0$, $\mathbf{f}_s = 0$, $\psi_0 = 0$, on Γ_m, $\mathbf{u}_s = (1, 0)^\top$, on Γ_{s_1}, $\mathbf{u}_s = (0, 0)^\top$, on Γ_{s_2}, and $\mathbf{u}_s = (1, 0)^\top$, on Γ_{s_3}.

For exhibiting the stochastic property of our problem, numerical solutions on the mesh $h_L = 1/64$ with four different samples of $\mathbb{K}(\omega, x)$ are shown in the Fig. 4, by using the flow speed and the velocity stream lines. From the comparison of the four solutions in the Fig. 4, one can see the randomness in the porous media and on the interface.

For the hierarchical quasi-uniform triangulation mesh $\{\mathcal{T}_\ell\}_{\ell=0}^L$, five levels are chosen, i.e., $h_\ell = \frac{2^{-\ell}}{4}$, $\ell = 0, 1, 2, 3, 4$ with $h_0 = 1/4$. An explicit numerical method is needed to determine the parameter γ in calculating $\{N_\ell^{\mathrm{ML}}\}_{\ell=0}^4$, which is needed for the MGMLMC method. Based on $C_\ell = \mathcal{O}(h_\ell^{-\gamma})$, $\ell = 0, 1, 2, 3$, we can compute γ after the computational cost $\{C_\ell\}_{\ell=0}^3$ of a few samples at every level are recorded. The cpu time and tic-toc time with different mesh size are shown in the Table 2, and the corresponding γ are 2.0536, 2.4549, which are illustrated in the Fig. 5. In this paper, we choose $\gamma = 2.4549$.

If the variance v_0 at the first level is known, the variance $\{v_\ell\}_{\ell=0}^L$ at the every level could be calculated by $v_\ell = \mathcal{O}(h_\ell^\beta)$, while the parameter β is approximated by the β of stochastic
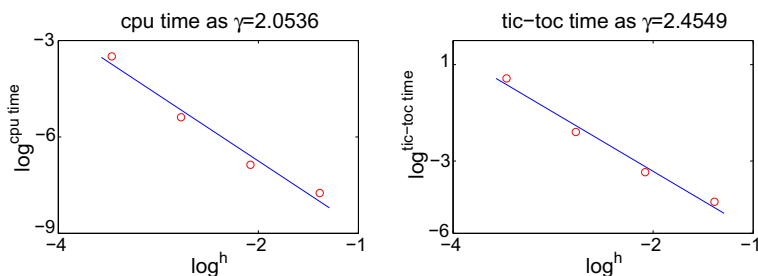
Fig. 5 γ of cpu time and tic-toc time

Table 3 Number of samples at every level

β	N_4^{SL}	N_0^{ML}	N_1^{ML}	N_2^{ML}	N_3^{ML}	N_4^{ML}
2.02	1277	4000	4000	1179	110	8
1.65	1352	4000	4000	2484	262	20
1.30	2221	4000	4000	4000	946	82

Table 4 The required error and the errors of numerical methods

β	Required Error	Error of SLMC	Error of MGMLMC
$2.02(\|\cdot\|_{L^2})$	4.00×10^{-4}	1.27×10^{-4}	1.82×10^{-4}
$1.65(\|\cdot\|_{L^\infty})$	1.20×10^{-3}	1.27×10^{-3}	1.69×10^{-3}
$1.30(\|\cdot\|_{H^1})$	1.20×10^{-3}	5.16×10^{-3}	8.77×10^{-3}

Darcy problem in the previous section. The variance v_0 at the first level is easy to be calculated with low computational cost.

Then using the formula (45) with the parameters β and γ we have gained, we can obtain the number of samples at every level based on the optimization problem (42) under the given sampling error e_L. In this experiment, the sampling error with each choice of β is given as the square of the required error in the Table 4. And the corresponding numbers of samples on every level are shown in the Table 3. Since we only generate 4000 samples of the hydraulic conductivity $K(\omega, x)$ in this experiment, the upper bound of the number of samples on every level is 4000.

For evaluating the accuracy of the SLMC method and the MGMLMC method, we generate the reference solution with the mesh size $h = 1/128$ and 4000 samples of hydraulic conductivity. Then the corresponding errors of the SLMC method and the MGMLMC method are shown in the Table 4, here these methods are performed with the number of samples in the Table 3. From the results in the Table 4, we can find that the errors of the SLMC method and the MGMLMC method have the same order of magnitude. In other words, these two numerical methods have the same accuracy.

To further numerically verify our claim that the MGMLMC method is as accurate as the SLMC method, we do the following process. At first, we calculate the numerical solution by the SLMC method with the mesh size $h_L = 1/64$, and record this solution. And we also use the MGMLMC method to gain another numerical solution with the same mesh size $h_L = 1/64$. Then, it is obvious that the difference between these two numerical solutions will indicate whether the MGMLMC method is as accurate as the SLMC method or not. A very simple way

Table 5 Relative errors of solutions by the SLMC method and the MGMLMC method

β	ϕ_m (%)	u_m^1 (%)	u_m^2 (%)	p_s (%)	u_s^1 (%)	u_s^2 (%)
2.02	1.63	1.32	0.42	0.03	0.01	0.02
1.65	1.98	1.54	1.84	0.01	0.04	0.02
1.30	3.26	3.11	8.30	0.01	0.02	0.02
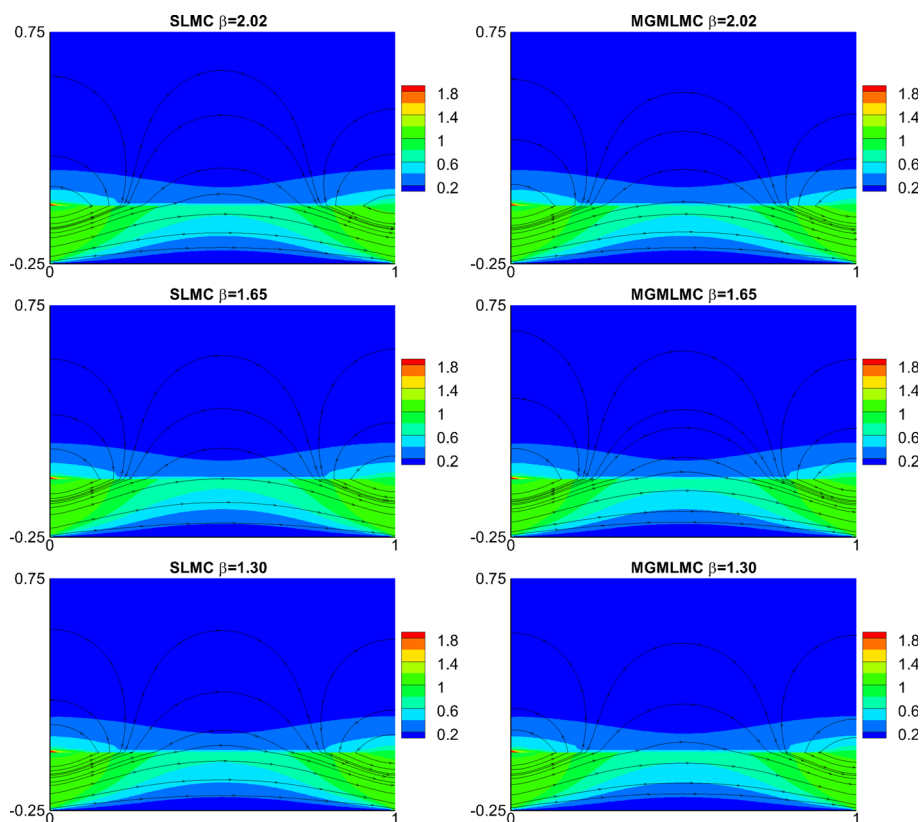
Fig. 6 Left: Numerical expectation of speed and stream lines by the SLMC method; Right: Numerical expectation of speed and stream lines by the MGMLMC method. Color represents the speed of flow

to estimate the difference between these two numerical solutions is to calculate their percent relative errors with a given norm, which are shown in the Table 5. Each row of the Table 5 is the percent relative errors with different choice of β, and each column of the Table 5 is the percent relative errors of the unknown parameters in our Stokes–Darcy model. We can find that the percent relative errors in the Table 5 are small, which indicates that the MGMLMC method is as accurate as the SLMC method. Furthermore, we exhibit the numerical solutions by these two methods with the mesh size $h_L = 1/64$ in the Fig. 6, which also shows that there is a slight difference between the numerical expectations of speed and stream lines by these two methods, and implies that the MGMLMC method is as accurate as the SLMC method. Moreover, an interesting finding through the Table 5 is that the percent relative errors of the parameters (p_s, u_s^1, u_s^2) in the Stokes equations are much smaller than the percent relative

Table 6 Efficiency of the MLMC and MGMLMC methods

β	T_c^{SL} (s)	T_c^{ML} (s)	T_c^{MGML} (s)	$T_c^{\mathrm{ML}}/T_c^{\mathrm{SL}}$ (%)	$T_c^{\mathrm{MGML}}/T_c^{\mathrm{SL}}$ (%)
2.02	1.68×10^7	1.57×10^5	2.53×10^4	0.93	0.15
1.65	1.78×10^7	3.62×10^5	3.80×10^4	2.04	0.21
1.30	2.92×10^7	1.35×10^6	7.24×10^4	4.64	0.25

errors of the parameters (ϕ_m, u_m^1, u_m^2) in Darcy system, which is corresponding to the setting that the random hydraulic conductivity is only a parameter in the Darcy domain and on the interface. Besides, based on the results in the Table 5, the MGMLMC method will be more accurate when the parameter β becomes larger. An explanation for this finding is given as follows. Through the results in the Table 3, we can find that more number of samples are required to capture the information in the probability space when the parameter β becomes smaller. But the upper bound of the number of samples on every level is fixed in this paper. Then there will be not enough information on the probability space in the performance of MGMLMC method when the parameter β becomes smaller. This finding also shows that how to determine the parameter β is one of the key points in the performance of MLMC method.

To illustrate the efficiency of the MLMC method and the MGMLMC method, the computational costs of the SLMC method, the MLMC method and the MGMLMC method are compared in the Table 6. Based on these results, it is easy to see that the MGMLMC method significantly reduce the computational cost with the same accuracy as the SLMC method.

6 Conclusion

In this paper, for the stochastic Stokes–Darcy interface model with random Beavers–Joseph interface condition, we proved the wellposedness of weak solution, and developed an accurate and efficient multigrid multilevel Monte Carlo method to solve the numerical approximations. For the MLMC method, a strategy is constructed to calculate the number of samples on every level. The computational cost is also analyzed and compared. By using the numerical examples, we verified the features of the numerical method and the theoretical conclusions.

Availability of Data and Materials The datasets generated during and/or analysed during the current study are available from the corresponding author on reasonable request.

Declarations

Conflict of interest The authors have no conflicts of interest to declare that are relevant to the content of this article.

Code Availability Custom code.

References

1. Arbogast, T., Gomez, M.: A discretization and multigrid solver for a Darcy–Stokes system of three dimensional Vuggy porous media. Comput. Geosci. **13**(3), 331–348 (2009)
2. Arbogast, T., Lehr, H.L.: Homogenization of a Darcy–Stokes system modeling Vuggy porous media. Comput. Geosci. **10**(3), 291–302 (2006)
3. Armentano, M.G., Stockdale, M.L.: Approximations by mini mixed finite element for the Stokes–Darcy coupled problem on curved domains. Int. J. Numer. Anal. Mod. **18**, 203–234 (2021)
4. Babuška, I., Gatica, G.N.: A residual-based a posteriori error estimator for the Stokes–Darcy coupled problem. SIAM J. Numer. Anal. **48**(2), 498–523 (2010)
5. Babuška, I., Nobile, F., Tempone, R.: A stochastic collocation method for elliptic partial differential equations with random input data. SIAM J. Numer. Anal. **45**(3), 1005–1034 (2007)
6. Babuška, I., Nobile, F., Tempone, R.: A stochastic collocation method for elliptic partial differential equations with random input data. SIAM Rev. **52**(2), 317–355 (2010)
7. Baccouch, M.: A finite difference method for stochastic nonlinear second-order boundary-value problems driven by additive noises. Int. J. Numer. Anal. Mod. **17**(3), 368–389 (2020)
8. Badea, L., Discacciati, M., Quarteroni, A.: Numerical analysis of the Navier–Stokes/Darcy coupling. Numer. Math. **115**(2), 195–227 (2010)
9. Bao, F., Cao, Y., Webster, C., Zhang, G.: A hybrid sparse-grid approach for nonlinear filtering problems based on adaptive-domain of the Zakai equation approximations. SIAM/ASA J. Uncertain. Quantif. **2**(1), 784–804 (2014)
10. Barenblatt, G.I., Zheltov, I.P., Kochina, I.N.: Basic concepts in the theory of seepage of homogeneous liquids in fissured rocks. J. Appl. Math. Mech. **24**(5), 1286–1303 (1960)
11. Barth, A., Schwab, C., Zollinger, N.: Multi-level Monte Carlo finite element method for elliptic PDEs with stochastic coefficients. Numer. Math. **199**(1), 123–161 (2011)
12. Beavers, G., Joseph, D.: Boundary conditions at a naturally permeable wall. J. Fluid Mech. **30**, 197–207 (1967)
13. Boubendir, Y., Tlupova, S.: Stokes–Darcy boundary integral solutions using preconditioners. J. Comput. Phys. **228**(23), 8627–8641 (2009)
14. Boubendir, Y., Tlupova, S.: Domain decomposition methods for solving Stokes–Darcy problems with boundary integrals. SIAM J. Sci. Comput. **35**(1), B82–B106 (2013)
15. Bramble, J.H.: Multigrid Methods, Pitman Research Notes in Mathematics Series, vol. 294. Longman Scientific & Technical, Harlow; copublished in the United States with John Wiley & Sons, Inc., New York (1993)
16. Brenner, S.C., Scott, L.R.: The Mathematical Theory of Finite Element Methods, 3rd edn. Springer, New York (1994)
17. Briggs, W.L., Henson, V.E., McCormick, S.F.: A Multigrid Tutorial, 2nd edn. Society for Industral and Appllied Mathematics, Philadelphia (2000)
18. Cai, M., Mu, M., Xu, J.: Numerical solution to a mixed Navier–Stokes–Darcy model by the two-grid approach. SIAM J. Numer. Anal. **47**(5), 3325–3338 (2009)
19. Camano, J., Gatica, G.N., Oyarzua, R., Ruiz-Baier, R., Venegas, P.: New fully-mixed finite element methods for the Stokes–Darcy coupling. Comput. Methods Appl. Mech. Eng. **295**, 362–395 (2015)
20. Cao, Y., Chu, Y., He, X.M., Wei, M.: Decoupling the stationary Navier-Stokes-Darcy system with the Beavers–Joseph–Saffman interface condition. Abstr. Appl. Anal. Article ID 136,483, 10 pages (2013)
21. Cao, Y., Gunzburger, M., He, X.M., Wang, X.: Robin-Robin domain decomposition methods for the steady Stokes–Darcy model with Beaver–Joseph interface condition. Numer. Math. **117**(4), 601–629 (2011)
22. Cao, Y., Gunzburger, M., He, X.M., Wang, X.: Parallel, non-iterative, multi-physics domain decomposition methods for time-dependent Stokes–Darcy systems. Math. Comput. **83**(288), 1617–1644 (2014)
23. Cao, Y., Gunzburger, M., Hu, X., Hua, F., Wang, X., Zhao, W.: Finite element approximation for Stokes–Darcy flow with Beavers–Joseph interface conditions. SIAM J. Numer. Anal. **47**(6), 4239–4256 (2010)
24. Cao, Y., Gunzburger, M., Hua, F., Wang, X.: Coupled Stokes–Darcy model with Beavers–Joseph interface boundary condition. Commun. Math. Sci. **8**(1), 1–25 (2010)
25. Çeşmelioğlu, A., Rivière, B.: Primal discontinuous Galerkin methods for time-dependent coupled surface and subsurface flow. J. Sci. Comput. **40**(1–3), 115–140 (2009)
26. Çeşmelioğlu, A., Rivière, B.: Existence of a weak solution for the fully coupled Navier-Stokes/Darcy-transport problem. J. Differ. Equations **252**(7), 4138–4175 (2012)
27. Charrier, J., Scheichl, R., Teckentrup, A.L.: Finite element error analysis of elliptic PDEs with random coefficients and its application to multilevel Monte Carlo methods. SIAM J. Numer. Anal. **51**(1), 322–352 (2013)

28. Chen, J., Sun, S., Wang, X.: A numerical method for a model of two-phase flow in a coupled free flow and porous media system. J. Comput. Phys. **268**, 1–16 (2014)
29. Chen, L., Hu, X., Wang, M., Xu, J.: A multigrid solver based on distributive smoother and residual overweighting for Oseen problems. Numer. Math. Theor. Methods Appl. **8**(2), 237–252 (2015)
30. Chen, W., Gunzburger, M., Hua, F., Wang, X.: A parallel Robin-Robin domain decomposition method for the Stokes–Darcy system. SIAM J. Numer. Anal. **49**(3), 1064–1084 (2011)
31. Chen, W., Gunzburger, M., Sun, D., Wang, X.: Efficient and long-time accurate second-order methods for the Stokes–Darcy system. SIAM J. Numer. Anal. **51**(5), 2563–2584 (2013)
32. Chidyagwai, P., Rivière, B.: On the solution of the coupled Navier–Stokes and Darcy equations. Comput. Methods Appl. Mech. Eng. **198**(47–48), 3806–3820 (2009)
33. Cushman, J.H.: The Physics of Fluids in Hierarchical Porous Media: Angstroms to Miles, vol. 10. Springer, Berlin (2013)
34. D'Angelo, C., Zunino, P.: Robust numerical approximation of coupled Stokes' and Darcy's flows applied to vascular hemodynamics and biochemical transport. ESAIM Math. Model. Numer. Anal. **45**(3), 447–476 (2011)
35. Diegel, A.E., Feng, X., Wise, S.M.: Analysis of a mixed finite element method for a Cahn–Hilliard–Darcy–Stokes system. SIAM J. Numer. Anal. **53**(1), 127–152 (2015)
36. Discacciati, M.: Domain decomposition methods for the coupling of surface and groundwater flows. Ph.D. thesis, Ecole Polytechnique Fédérale de Lausanne, Switzerland (2004)
37. Discacciati, M., Gerardo-Giorda, L.: Optimized Schwarz methods for the Stokes–Darcy coupling. IMA J. Numer. Anal. **38**(4), 1959–1983 (2018)
38. Discacciati, M., Miglio, E., Quarteroni, A.: Mathematical and numerical models for coupling surface and groundwater flows. Appl. Numer. Math. **43**(1–2), 57–74 (2002)
39. Discacciati, M., Quarteroni, A.: Convergence analysis of a subdomain iterative method for the finite element approximation of the coupling of Stokes and Darcy equations. Comput. Vis. Sci. **6**(2–3), 93–103 (2004)
40. Discacciati, M., Quarteroni, A., Valli, A.: Robin-Robin domain decomposition methods for the Stokes–Darcy coupling. SIAM J. Numer. Anal. **45**(3), 1246–1268 (2007)
41. Dostert, P., Efendiev, Y., Hou, T.Y.: Multiscale finite element methods for stochastic porous media flow equations and application to uncertainty quantification. Comput. Method Appl. M. **197**(43–44), 3445–3455 (2008)
42. Douglas, C.C., Hu, X., Bai, B., He, X.M., Wei, M., Hou, J.: A data assimilation enabled model for coupling dual porosity flow with free flow. In: 17th International Symposium on Distributed Computing and Applications for Business Engineering and Science (DCABES), Wuxi, China, October 19–23, 2018, pp. 304–307 (2018)
43. Drzisga, D., Gmeiner, B., Rüde, U., Scheichl, R., Wohlmuth, B.: Scheduling massively parallel multigrid for multilevel Monte Carlo methods. SIAM J. Sci. Comput. **39**(5), S873–S897 (2017)
44. Ervin, V.J., Jenkins, E.W., Lee, H.: Approximation of the Stokes–Darcy system by optimization. J. Sci. Comput. **59**(3), 775–794 (2014)
45. Ervin, V.J., Jenkins, E.W., Sun, S.: Coupled generalized nonlinear Stokes flow with flow through a porous medium. SIAM J. Numer. Anal. **47**(2), 929–952 (2009)
46. Evans, L.C.: Partial Differential Equations, Graduate Studies in Mathematics, vol. 19, 2nd edn. American Mathematical Society, Providence (2010)
47. Feng, W., He, X.M., Wang, Z., Zhang, X.: Non-iterative domain decomposition methods for a non-stationary Stokes–Darcy model with Beavers-Joseph interface condition. Appl. Math. Comput. **219**(2), 453–463 (2012)
48. Galvis, J., Sarkis, M.: Non-matching mortar discretization analysis for the coupling Stokes–Darcy equations. Electron. Trans. Numer. Anal. **26**, 350–384 (2007)
49. Ganis, B., Klie, H., Wheeler, M.F., Wildey, T., Yotov, I., Zhang, D.: Stochastic collocation and mixed finite elements for flow in porous media. Comput. Method Appl. M. **197**(43–44), 3547–3559 (2008)
50. Gao, Y., He, X.M., Mei, L., Yang, X.: Decoupled, linear, and energy stable finite element method for the Cahn–Hilliard–Navier–Stokes–Darcy phase field model. SIAM J. Sci. Comput. **40**(1), B110–B137 (2018)
51. Gatica, G.N., Meddahi, S., Oyarzúa, R.: A conforming mixed finite-element method for the coupling of fluid flow with porous media flow. IMA J. Numer. Anal. **29**(1), 86–108 (2009)
52. Ghanem, R., Dham, S.: Stochastic finite element analysis for multiphase flow in heterogeneous porous media. Transport Porous Med. **32**(3), 239–262 (1998)
53. Giles, M.B.: Improved multilevel Monte Carlo convergence using the Milstein scheme. In: Monte Carlo and Quasi-Monte Carlo Methods, 2006, pp. 343–358. Springer, Berlin (2008)
54. Giles, M.B.: Multilevel Monte Carlo path simulation. RAIRO-Oper. Res. **56**, 607–617 (2008)

55. Giles, M.B.: Multilevel Monte Carlo methods. Acta Numer. **24**(1), 259–328 (2015)
56. Girault, V., Raviart, P.A.: Finite Element Methods for Navier–Stokes Equations: Theory and Algorithms, Springer Series in Computational Mathematics, vol. 5. Springer, Berlin (1986)
57. Girault, V., Rivière, B.: DG approximation of coupled Navier–Stokes and Darcy equations by Beaver–Joseph–Saffman interface condition. SIAM J. Numer. Anal. **47**(3), 2052–2089 (2009)
58. Girault, V., Vassilev, D., Yotov, I.: Mortar multiscale finite element methods for Stokes–Darcy flows. Numer. Math. **127**(1), 93–165 (2014)
59. Graham, I.G., Huo, F.Y., Nuyens, D., Scheichl, R., Sloan, I.H.: Quasi-Monte Carlo methods for elliptic PDEs with random coefficients and applications. J. Comput. Phys. **230**(10), 3668–3694 (2011)
60. Gunzburger, M., He, X.M., Li, B.: On Ritz projection and multi-step backward differentiation schemes in decoupling the Stokes–Darcy model. SIAM J. Numer. Anal. **56**(1), 397–427 (2018)
61. Guo, C., Wang, J., Wei, M., He, X.M., Bai, B.: Multi-stage fractured horizontal well numerical simulation and its application in tight shale reservoirs. SPE-176714, SPE Russian Petroleum Technology Conference, Moscow, Russia, October 26–28 (2015)
62. Han, D., He, X.M., Wang, Q., Wu, Y.: Existence and weak-strong uniqueness of solutions to the Cahn–Hilliard–Navier–Stokes–Darcy system in superposed free flow and porous media. Nonlinear Anal. **211**, #112,411 (2021)
63. Han, D., Sun, D., Wang, X.: Two-phase flows in karstic geometry. Math. Methods Appl. Sci. **37**(18), 3048–3063 (2014)
64. Hanspal, N., Waghode, A., Nassehi, V., Wakeman, R.: Numerical analysis of coupled Stokes/Darcy flow in industrial filtrations. Transport Porous Med. **64**, 73–101 (2006)
65. He, X.M., Jiang, N., Qiu, C.: An artificial compressibility ensemble algorithm for a stochastic Stokes–Darcy model with random hydraulic conductivity and interface conditions. Int. J. Numer. Methods Eng. **121**(4), 712–739 (2020)
66. He, X.M., Li, J., Lin, Y., Ming, J.: A domain decomposition method for the steady-state Navier–Stokes–Darcy model with Beavers–Joseph interface condition. SIAM J. Sci. Comput. **37**(5), S264–S290 (2015)
67. Hoppe, R., Porta, P., Vassilevski, Y.: Computational issues related to iterative coupling of subsurface and channel flows. Calcolo **44**(1), 1–20 (2007)
68. Hou, J., Qiu, M., He, X.M., Guo, C., Wei, M., Bai, B.: A dual-porosity-Stokes model and finite element method for coupling dual-porosity flow and free flow. SIAM J. Sci. Comput. **38**(5), B710–B739 (2016)
69. Igreja, I., Loula, A.F.D.: A stabilized hybrid mixed DGFEM naturally coupling Stokes–Darcy flows. Comput. Methods Appl. Mech. Eng. **339**, 739–768 (2018)
70. Jiang, N., Qiu, C.: An efficient ensemble algorithm for numerical approximation of stochastic Stokes–Darcy equations. Comput. Methods Appl. Mech. Eng. **343**, 249–275 (2019)
71. Kanschat, G., Riviére, B.: A strongly conservative finite element method for the coupling of Stokes and Darcy flow. J. Comput. Phys. **229**, 5933–5943 (2010)
72. Karper, T., Mardal, K.A., Winther, R.: Unified finite element discretizations of coupled Darcy–Stokes flow. Numer. Methods Part. D. E. **25**(2), 311–326 (2009)
73. Kornhuber, R., Schwab, C., Wolf, M.W.: Multilevel Monte Carlo finite element methods for stochastic elliptic variational inequalities. SIAM J. Numer. Anal. **52**(3), 1243–1268 (2014)
74. Kubacki, M., Moraiti, M.: Analysis of a second-order, unconditionally stable, partitioned method for the evolutionary Stokes–Darcy model. Int. J. Numer. Anal. Model. **12**(4), 704–730 (2015)
75. Kumar, P., Oosterlee, C.W., Dwight, R.P.: A multigrid multilevel Monte Carlo method using high-order finite-volume scheme for lognormal diffusion problems. Int. J. Uucertain. Quan. **7**(1), 57–81 (2017)
76. Kumara, P., Luo, P., Gaspara, F.J., Oosterleea, C.W.: A multigrid multilevel Monte Carlo method for transport in the Darcy–Stokes system. J. Comput. Phys. **371**, 382–408 (2018)
77. Kuo, F.Y., Schwab, C., Sloan, I.H.: Multi-level quasi-Monte Carlo finite element methods for a class of elliptic PDEs with random coefficients. Found. Comput. Math. **15**(2), 411–449 (2015)
78. Layton, W., Tran, H., Trenchea, C.: Analysis of long time stability and errors of two partitioned methods for uncoupling evolutionary groundwater-surface water flows. SIAM J. Numer. Anal. **51**(1), 248–272 (2013)
79. Layton, W.J., Schieweck, F., Yotov, I.: Coupling fluid flow with porous media flow. SIAM J. Numer. Anal. **40**(6), 2195–2218 (2002)
80. Li, H., Zhang, D.: Probabilistic collocation method for flow in porous media: Comparisons with other stochastic methods. Water Resour. Res. **43**(9) (2007)
81. Li, R., Li, J., He, X.M., Chen, Z.: A stabilized finite volume element method for a coupled Stokes–Darcy problem. Appl. Numer. Math. **133**, 2–24 (2018)
82. Lipnikov, K., Vassilev, D., Yotov, I.: Discontinuous Galerkin and mimetic finite difference methods for coupled Stokes–Darcy flows on polygonal and polyhedral grids. Numer. Math. **126**(2), 321–360 (2014)

83. Liu, Y., He, Y., Li, X., He, X.M.: A novel convergence analysis of Robin-Robin domain decomposition method for Stokes–Darcy system with Beavers–Joseph interface condition. Appl. Math. Lett. **119**, #107,181 (2021)

84. Mahbub, M.A.A., He, X.M., Nasu, N.J., Qiu, C., Wang, Y., Zheng, H.: A coupled multi-physics model and a decoupled stabilized finite element method for closed-loop geothermal system. SIAM J. Sci. Comput. **42**(4), B951–B982 (2020)

85. Mahbub, M.A.A., He, X.M., Nasu, N.J., Qiu, C., Zheng, H.: Coupled and decoupled stabilized mixed finite element methods for non-stationary dual-porosity-Stokes fluid flow model. Int. J. Numer. Methods Eng. **120**(6), 803–833 (2019)

86. Márquez, A., Meddahi, S., Sayas, F.J.: Strong coupling of finite element methods for the Stokes–Darcy problem. IMA J. Numer. Anal. **35**(2), 969–988 (2015)

87. Mu, M., Xu, J.: A two-grid method of a mixed Stokes–Darcy model for coupling fluid flow with porous media flow. SIAM J. Numer. Anal. **45**(5), 1801–1813 (2007)

88. Mu, M., Zhu, X.: Decoupled schemes for a non-stationary mixed Stokes–Darcy model. Math. Comput. **79**(270), 707–731 (2010)

89. Münzenmaier, S., Starke, G.: First-order system least squares for coupled Stokes–Darcy flow. SIAM J. Numer. Anal. **49**(1), 387–404 (2011)

90. Muzhinji, K., Shateyi, S., Motsa, S.S.: The mixed finite element multigrid method for Stokes equations. Sci. World J. 1–12 (2015)

91. Najm, H.N.: Uncertainty quantification and polynomial chaos techniques in computational fluid dynamics. Annu. Rev. Fluid Mech. **41**, 35–52 (2009)

92. Nobile, F., Tempone, R., Webster, C.G.: An anisotropic sparse grid stochastic collocation method for partial differential equations with random input data. SIAM J. Numer. Anal. **46**(5), 2411–2442 (2008)

93. Nobile, F., Tempone, R., Webster, C.G.: A sparse grid stochastic collocation method for partial differential equations with random input data. SIAM J. Numer. Anal. **46**(5), 2309–2345 (2008)

94. Nouri, K., Ranjbar, H., López, J.C.C.: Modifying the split-step θ-method with harmonic-mean term for stochastic differential equations. Int. J. Numer. Anal. Mod. **17**, 662–678 (2020)

95. Qiu, C., He, X.M., Li, J., Lin, Y.: A domain decomposition method for the time-dependent Navier–Stokes–Darcy model with Beavers–Joseph interface condition and defective boundary condition. J. Comput. Phys. **411**, #109,400 (2020)

96. Quarteroni, A., Valli, A.: Numerical Approximation of Partial Differential Equations, Springer Series in Computational Mathematics, vol. 23. Springer, Berlin (1994)

97. Rivière, B., Yotov, I.: Locally conservative coupling of Stokes and Darcy flows. SIAM J. Numer. Anal. **42**(5), 1959–1977 (2005)

98. Robbe, P., Nuyens, D., Vandewalle, S.: Recycling samples in the multigrid multilevel (quasi-)Monte Carlo method. SIAM J. Sci. Comput. **41**(5), S37–S60 (2019)

99. Robert, C.P., Casella, G.: Monte Carlo Statistical Methods, 2nd edn. Springer, New York (2004)

100. Rui, H., Zhang, J.: A stabilized mixed finite element method for coupled Stokes and Darcy flows with transport. Comput. Methods Appl. Mech. Engrg. **315**, 169–189 (2017)

101. Rui, H., Zhang, R.: A unified stabilized mixed finite element method for coupling Stokes and Darcy flows. Comput. Methods Appl. Mech. Eng. **198**(33–36), 2692–2699 (2009)

102. Rybak, I., Magiera, J.: A multiple-time-step technique for coupled free flow and porous medium systems. J. Comput. Phys. **272**(272), 327–342 (2014)

103. Shan, L., Zheng, H.: Partitioned time stepping method for fully evolutionary Stokes–Darcy flow with Beavers–Joseph interface conditions. SIAM J. Numer. Anal. **51**(2), 813–839 (2013)

104. Smith, R.C.: Uncertainty Quantification: Theory, Implementation, and Applications, Computational Science and Engineering, vol. 12. SIAM, Philadelphia (2013)

105. Stoter, S.K.F., Müller, P., Cicalese, L., Tuveri, M., Schillinger, D., Hughes, T.J.R.: A diffuse interface method for the Navier–Stokes/Darcy equations: perfusion profile for a patient-specific human liver based on MRI scans. Comput. Methods Appl. Mech. Eng. **321**, 70–102 (2017)

106. Strang, G.: Computational Science and Engineering, vol. 791. Wellesley-Cambridge Press, Wellesley (2007)

107. Teckentrup, A.L., Scheichl, R., Giles, M.B., Ullmann, E.: Further analysis of multilevel Monte Carlo methods for elliptic PDEs with random coefficients. Numer. Math. **125**(3), 569–600 (2013)

108. Trottenberg, U., Oosterlee, C.W., Schüller, A.: Multigrid. With contributions by A. Brandt, P. Oswald and K. Stüben. Academic Press, Inc., San Diego, CA (2001)

109. Vassilev, D., Wang, C., Yotov, I.: Domain decomposition for coupled Stokes and Darcy flows. Comput. Methods Appl. Mech. Eng. **268**, 264–283 (2014)

110. Vassilev, D., Yotov, I.: Coupling Stokes-Darcy flow with transport. SIAM J. Sci. Comput. **31**(5), 3661–3684 (2009)

111. Wang, D., Cao, Y., Li, Q., Shen, J.: A stochastic gradient descent method for the design of optimal random interface in thin-film solar cells. Int. J. Numer. Anal. Mod. **18**, 384–398 (2021)

112. Wang, G., Wang, F., Chen, L., He, Y.: A divergence free weak virtual element method for the Stokes–Darcy problem on general meshes. Comput. Methods Appl. Mech. Eng. **344**, 998–1020 (2019)

113. Wang, M., Chen, L.: Multigrid methods for the stokes equations using distributive Gauss–Seidel relaxations based on the least squares commutator. J. Sci. Comput. **56**(2), 409–431 (2013)

114. Wang, W., Xu, C.: Spectral methods based on new formulations for coupled Stokes and Darcy equations. J. Comput. Phys. **257, part A**, 126–142 (2014)

115. Wei, X., Zhao, J., He, X.M., Hu, Z., Du, X., Han, D.: Adaptive Kriging method for uncertainty quantification of the photoelectron sheath and dust levitation on the lunar surface. J. Verif. Valid. Uncert. **6**(1), #011,006 (2021)

116. Wu, K., Tang, H., Xiu, D.: A stochastic Galerkin method for first-order quasilinear hyperbolic systems with uncertainty. J. Comput. Phys. **345**, 224–244 (2017)

117. Xiu, D., Karniadakis, G.E.: Modeling uncertainty in steady state diffusion problems via generalized polynomial chaos. Comput. Methods Appl. Mech. Eng. **191**(43), 4927–4948 (2002)

118. Xiu, D., Karniadakis, G.E.: The Wiener-Askey polynomial chaos for stochastic differential equations. SIAM J. Sci. Comput. **24**(2), 619–644 (2002)

119. Zhang, D., Guo, L., Karniadakis, G.E.: Learning in modal space: solving time-dependent stochastic PDEs using physics-informed neural networks. SIAM J. Sci. Comput. **42**(2), A639–A665 (2020)

120. Zhang, D., Lu, Z.: An efficient, high-order perturbation approach for flow in random porous media via Karhunen-Loève and polynomial expansions. Numer. Math-Theory Methods **194**(2), 773–794 (2004)

121. Zhang, J., Rui, H., Cao, Y.: A partitioned method with different time steps for coupled Stokes and Darcy flows with transport. Int. J. Numer. Anal. Mod. **16**, 463–498 (2019)

122. Zhang, Y., Zhou, C., Qu, C., Wei, M., He, X.M., Bai, B.: Fabrication and verification of a glass-silicon-glass micro-nanofluidic model for investigating multi-phase flow in unconventional dual-porosity porous media. Lab Chip **19**, 4071–4082 (2019)

123. Zhang, Z., Rozovskii, B., Karniadakis, G.E.: Strong and weak convergence order of finite element methods for stochastic PDEs with spatial white noise. Numer. Math. **134**(1), 61–89 (2016)

124. Zhao, B., Zhang, M., Liang, C.: Global well-posedness for Navier–Stokes–Darcy equations with the free interface. Int. J. Numer. Anal. Mod. **18**, 569–619 (2021)

125. Zhao, J., Wei, X., Hu, Z., He, X.M., Han, D.: Photoelectron sheath near the lunar surface: fully kinetic modeling and uncertainty quantification analysis, #AIAA 2020-1548. In: Proceeding of AIAA Scitech 2020 Forum, Orlando, Florida, January 6–10 (2020)

Authors and Affiliations

Zhipeng Yang[1,2] · Ju Ming[3] · Changxin Qiu[4] · Maojun Li[5] · Xiaoming He[6]

✉ Ju Ming
jming@hust.edu.cn

Zhipeng Yang
yangzp2020@mail.sustech.edu.cn

Changxin Qiu
qiuchangxin@nbu.edu.cn

Maojun Li
limj@uestc.edu.cn

Xiaoming He
hex@mst.edu

1   Department of Mathematics, Southern University of Science and Technology, Shenzhen 518055, People's Republic of China

2 Division of Applied and Computational Mathematics, Beijing Computational Science Research Center, Beijing 100094, People's Republic of China

3 School of Mathematics and Statistics, Huazhong University of Science and Technology, Wuhan 430074, People's Republic of China

4 School of Mathematics and Statistics, Ningbo University, Ningbo 315211, People's Republic of China

5 School of Mathematical Sciences, University of Electronic Science and Technology of China, Chengdu 611731, Sichuan, People's Republic of China

6 Department of Mathematics and Statistics, Missouri University of Science and Technology, Rolla, MO 65409, USA